Synthesis of pyridyl pyrimidine hedgehog signaling pathway inhibitors and their antitumor activity in human pancreatic cancer

Hongjuan Li, Miao Wang, Shu Han, Fangliang Yang, Youbing Wang, Ge Jin, Chiyu Sun

PII: S0223-5234(24)00842-0

DOI: https://doi.org/10.1016/j.ejmech.2024.116961

Reference: EJMECH 116961

To appear in: *European Journal of Medicinal Chemistry*

Received Date: 29 May 2024

Revised Date: 9 October 2024

Accepted Date: 11 October 2024

Please cite this article as: H. Li, M. Wang, S. Han, F. Yang, Y. Wang, G. Jin, C. Sun, Synthesis of pyridyl pyrimidine hedgehog signaling pathway inhibitors and their antitumor activity in human pancreatic cancer, *European Journal of Medicinal Chemistry*, https://doi.org/10.1016/j.ejmech.2024.116961.

Synthesis of pyridyl pyrimidine hedgehog signaling pathway inhibitors and their antitumor activity in human pancreatic cancer

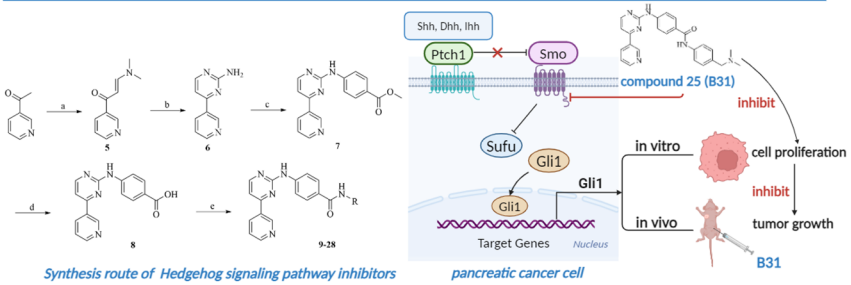

Synthesis route of Hedgehog signaling pathway inhibitors *pancreatic cancer cell*

Conflusion : A series of novel pyridyl pyrimidine hedgehog inhibitors has been synthesized. Among them, B31 stands out for its superior Hh pathway inhibition and robust Smo binding affinity. Additionally, B31 achieves a remarkable 82% reduction in tumor volume in pancreatic cancer models.

Synthesis of pyridyl pyrimidine hedgehog signaling pathway inhibitors and their antitumor activity in human pancreatic cancer

Hongjuan Li,[a] Miao Wang,[a] Shu Han,[a] Fangliang Yang,[b] Youbing Wang,[b] Ge Jin,[b] Chiyu Sun*[a,b]

[a]School of Basic Medical Sciences, Shenyang Medical College, Shenyang 110034, China

[b]School of Pharmacy, Shenyang Medical College, Shenyang 110034, China

Pancreatic cancer (PC) is an extremely lethal malignant tumor. The Hedgehog (Hh) signaling pathway is implicated in embryonic development, regulation of tumor stem cells, and modulation of the tumor microenvironment. Aberrant activation of Hh pathway leads to the development of multiple malignant tumors, especially Hh-driven PC. Targeting the molecular regulation of the Hh signaling pathway presents a promising therapeutic strategy for PC treatment. Hence, there is a high demand for novel molecules that inhibit the Hh pathway. In this study, the Hh pathway inhibitors bearing pyridyl pyrimidine skeleton were designed, synthesized, and characterized. Among them, N-(4-((dimethylamino)methyl)phenyl)-4-((4-(pyridin-3-yl)pyrimidin-2-yl)amino)benzamide (B31) emerged as the most potent analog following screening with a Gli luciferase reporter assay, competing with cyclopamine in the binding site of Smo protein. Molecular simulation revealed that B31 interacts with Smo through hydrogen bonds, hydrophobic interactions, and electrostatic forces. B31 inhibited PC cell proliferation, migration, and induced apoptosis by suppressing Gli1 expression at both the transcriptional and translational levels. Moreover, B31 significantly regressed subcutaneous tumors formed by BxPC-3 cells in nude mice without inducing toxic effects. These results underscore the enhanced efficacy of B31 in the PC model and offer a new avenue for developing effective Hh pathway inhibitors for clinical PC treatment.

Keyword: Pancreatic cancer, Hedgehog signaling pathway, Pyrimidine, Synthesis, Proliferation

1.Introduction

Pancreatic cancer (PC) is a highly fatal malignancy, and despite a general decline in cancer mortality rates, its treatment remains fraught with numerous challenges. According to the latest cancer statistics, PC is the third leading cause of cancer-related deaths. With its propensity for local advancement and metastatic phenotypes, the 5-year survival rate for PC stands at mere 4%[1-3]. Typically, PC lacks noticeable symptoms in its early stages, often presenting with local or distant metastases by the time of diagnosis, which precludes opportunities for curative surgery. Currently, effective treatment options for pancreatic cancer are exceedingly limited. Patients who undergo surgical resection often require adjuvant therapy with appropriate drugs, however, postoperative mortality and recurrence rates remain unacceptably high[4-6]. With the expanding understanding of PC biology and related disciplines, the development of drugs targeting specific cell signaling pathways has emerged as a promising alternative for treating PC patients. Reports indicate that the occurrence and progression of PC are associated with the abnormal activation of multiple signaling

pathways, including Hedgehog (Hh)[7], Notch[8,9], Wnt[10,11], NF-κB[12,13], PI3K-Akt[14], HGF/c-Met[15,16], and FGFR[17,18].

The Hh signaling pathway exerts a major influence on the modulation of cellular growth, proliferation, and stem cell maintenance. Insufficiency of Hh signaling results in developmental imperfections, however, its overactivation is associated with PC[19], basal cell carcinoma (BCC)[20], medulloblastoma (MB)[21], acute myeloid leukemia (AML)[22,23], as well as colon and prostate cancer[24,25]. Abnormal activation of Hh signaling involves patched (Ptch) mutations and ligand-dependent mechanisms[26]. The activation of Hh signaling is derived from the direct binding between Hh ligand and Ptch, which relieves its suppression of smoothened (Smo). In turn, Smo translocates to the primary cilium and initiates Glioma-associated oncogene homologue (Gli)-dependent transcription of Hh target genes, including Gli1, Ptch1, cyclin D1,and N-myc[27,28]. Hence, inhibiting abnormal Hh signaling reveals a promising and effective method for cancer treatment.

Smo has been a primary target in the development of Hh signaling pathway inhibitors for decades[29]. Moreover, its suppression leads to the down-regulation of genes related to tumor growth and progression. Vismodegib (**1**), Sonidegib (**2**) and Glasdegib (**3**) as Smo inhibitors have been authorized by the FDA for the treatment of BCC and AML so far (Figure 1)[30-33]. Many other compounds, such as Taladegib, Vitamin D3, Itraconazole and LEQ506, are in different clinical phases[34-37]. In the clinical Phase II trial for PC, the results of compound **1** were unsatisfactory. For instance, although compound **1** inhibited Hh signaling transduction by downregulating Hh target genes, there was no significant difference in overall and progression-free survival between patients treated with compound **1**, whether with or without gemcitabine[38]. Furthermore, there was no evident advantage of the combination group compared to gemcitabine alone, probably in virtue of its relatively low efficacy in blocking Hh signaling in PC[39]. Also, adverse effects, including diarrhea, weight loss, muscle spasms, and taste disturbances, occurred in a large number of patients treated with compound **1**[40]**.** Additionally, acquired resistance resulting from Smo mutations hindered its continued advancement[41,42]. It is credible that the advancement of compounds with novel structures targeting the Smo protein will distinctly improve the effectiveness of PC treatment.

Figure 1 should be here

Figure 1 The launched inhibitors of the Hh signaling pathway

In collaboration with Exelixis, Bristol-Myers-Squibb has investigated a series of quinazoline Hh pathway inhibitors. Among all the derivatives, BMS-833923 (**4**) dramatically reduced the mRNA expression of Gli1 and Ptch1 and inhibited the proliferation of several cancer cell lines[43,44]. Compound **4** was advanced to Phase I clinical trials in combination with Dasatinib for the treatment of chronic myelogenous leukemia, however, compound **4** was withdrawn due to unsatisfactory efficacy[45]. Our efforts for further structural optimization were guided by its large rigidity. Pyrimidine is more flexible and occupies less space compared with quinazoline. Besides,

pyrimidine is a well-known pharmacophore with various biological activities, such as neurodegenerative diseases, anticancer, anti-inflammation, antibacterial, and antitubercular activities[46,47]. We envision that replacing quinazoline with pyrimidine in our target compounds will retain antitumor activity. Pyridine is a water-soluble group and often acts as hydrogen bonds acceptor in drug design. For instance, Nilotinib and Crizotinib bearing pyridyl showed better curative effect in the therapy of chronic myeloid leukemia and non-small cell lung cancer[48,49]. Hence, introducing a pyridine group at the 4-position of the pyrimidine increases the hydrophilicity. An aniline group linked to the 2-position of the pyrimidine maintains appropriate hydrophobic interactions. In addition, diverse aniline formyl groups were added as tail parts to adjust their lipid-water partition coefficient. (Figure 2). Therefore, novel compounds with a pyridyl pyrimidine scaffold were prepared and their Hh pathway inhibition was evaluated. Subsequently, B31 was further investigated for its competitive binding to Smo using a fluorescence probe assay, and its pharmacological evaluation was conducted at both cellular and animal levels to explore its anti-PC effectiveness.

Figure 2 should be here

Figure 2 Design of the pyridyl pyrimidine derivatives

2. Results and Discussion

2.1 Chemistry

The synthetic routes of the target compounds were summarized in Scheme 1. 3-Acetylpyridine was coupled with N,N-dimethylformamide dimethylacetal via nucleophilic addition-elimination in xylene to give compound **5**, which was converted to the key intermediate **6** through its cyclization with guanidine in n-butanol. Then, methyl 4-bromobenzoate was reacted with **6** to obtain compound **7** under nitrogen atmosphere via Buchwald-Hartwig cross coupling. In alkaline conditions, the ester **7** was rapidly hydrolyzed to the carboxylic acid **8** in refluxing aqueous alcohol. Finally, the condensation of **8** with different arylamines afforded the target compounds **9**–**28**.

Scheme 1 should be here

Scheme 1 Reagents and conditions: (a) $(CH_3)_2NCH(OCH_3)_2$, xylene, 140℃, 20h, yield 63%; (b) guanidine hydrochloride, NaOH, n-butanol, reflux, 12h, yield 69%; (c) methyl 4-bromobenzoate, $Pd(OAc)_2$, BINAP, Cs_2CO_3, dioxane, under N_2, reflux, 24 h, yield 88%; (d) NaOH, aqueous alcohol, reflux, 2 h, yield 87%; (e) different aniline, HATU, DIPEA, DMF, r.t., 24 h, yield 46-81%.

2.2 The inhibition of the Hh signaling pathway by pyridyl pyrimidine analogs.

The pyridyl pyrimidine analogs **9**-**28** were estimated inhibition of the Hh signaling pathway using a Gli luciferase reporter assay. Compound **1** and **4** were used as the positive control and lead compound, respectively. And the results expressed as IC_{50} values were outlined in Table 1.

Table 1 should be here

Table 1 Structure activity relationship (SAR) of target compounds

Trifluoromethyl analog **10** or fluoro analog **11** exhibited higher potency as compared to the pyridine derivative **9**. When fluorine was retained at meta-position of benzene ring, the meta-methyl derivative (**14**, IC_{50} = 10.3 nM) showed higher activity compared to the para-methyl and para-morpholine analogs (**12** and **13**). If the fluorine at meta-position is removed, its anti-Hh activity decreases (**15** vs. **14**). The potency of the monomethoxyl-substituted **17** at the ortho-position was superior to that of the methyl substituted **16**. However, diminished activity was observed when the methoxyl was transferred to the para-position on the phenyl ring (**18** vs. **17**). Although poly-methoxyl substituents such as **19**, **20** and **21** were effective against Hh signaling, their IC_{50} values were higher than that of the mono-substituted **18**. When other electron-donating groups were added at the para-position, the N-methylpiperazine derivative (**24**, IC_{50} = 4.5 nM) and the N,N-dimethylamino methylene derivative (**25**, IC_{50} = 2.7 nM) were more potent compared to the ethoxy and the morpholine analogs (**22** and **23**). Yet, the electron-withdrawing groups such as para-trifluoromethyl, para-fluoro, and para-chlorine analogs (**26**, **27** and **28**) were less potent than the analogs with electron-donating groups discussed above. Overall, compound **25** (**B31**) displayed the most potent Hh inhibition in this class. Most interestingly, its potency was 2-fold higher than the lead compound **4** and 5.5-fold higher than the launched compound **1**.

In order to explore whether B31 is an antagonist acting on the Smo protein, a fluorescent cyclopamine-based competitive binding assay was developed (Figure 3). After incubation with BODIPY-cyclopamine, the Smo protein bound to cyclopamine on the cell membrane exhibited distinct green fluorescence. Compared with compound **1**, B31 exhibited similar fluorescence quenching after co-incubation with itself. Moreover, the fluorescence intensity faded with the increasing concentration of B31, indicating that B31 was a competitive antagonist of cyclopamine binding to Smo protein. The interactions involved include hydrogen bonds, hydrophobic interactions, and electrostatic forces.

Figure 3 should be here.

Figure 3 BODIPY-cyclopamine competitive binding assay based on Smo-297T cells. Scale bar=100 μm.

A molecular docking study was conducted to analyze the binding mode of target compounds with Smo protein (PDB ID: 5L7I). As presented in Figure 4A, the binding orientations of B31 overlapped well with those of compound **1**. In the binding mode (Figure 4B), the nitrogen atom of pyridine and the hydrogen atom of the nitrogen methyl group in B31 formed hydrogen bonds with Arg400, Lys395 and Glu481, respectively. B31 and Glu518 formed a π-anion electrostatic interaction. Besides, each aromatic ring of B31 engaged in alkyl or π hydrophobic interactions with Leu522, Met230, Pro513, and Phe484. The computational simulation interpreted the preferential inhibition of Smo by B31 at the molecular level.

Figure 4 should be here

Figure 4 Schematic diagram of molecular docking results. (A) Overlay of B31 (yellow) and vismodegib (green) in the binding pocket of Smo. (B) Docking conformation of B31 at the binding site. Hydrogen bonds are indicated by dashed green lines. Electrostatic force are shown by dashed orange lines. Hydrophobic interactions are represented by dashed pink lines. Amino acids in the vicinity are shown in gray stick format and labeled.

2.3 In vitro antitumor activity of B31

The aberrant activation of Hh signaling is closely associated with PC, hence the antiproliferative activity of B31 on PC cell lines was evaluated by MTT assay. The cell viabilities of PANC-1 and BxPC-3 cells apparently dropped when treated with gradually increasing concentrations of B31 (Figure 5). The IC_{50} value of B31 for PANC-1 cells was 4.204 ± 0.687 μM, and for BxPC-3 cells was 3.570 ± 0.127 μM. These values are 2.5-fold and 3-fold higher than those of compound **4**, respectively, and 12-fold and 10-fold higher than those of compound **1.**

Figure 5 should be here

Figure 5 (A, B) Cell cytotoxicity assay of PANC-1 and BxPC-3 cells treated with Vismodegib compound **4**, and B31. Cell viability was evaluated by MTT assay. Data is presented as the mean ± S.D. of three separate experiments (*P < 0.05, **P < 0.01, ***P < 0.001 vs. Vismodegib; $^{\#}$P < 0.05, $^{\#\#}$P < 0.01, $^{\#\#\#}$P < 0.001 vs.compound **4**, n=3).

Since BxPC-3 and PANC-1 cells express high levels of Hh signaling pathway components, Western blot results indicated a dose-dependent reduction of Gli1 in these cells after B31 treatment (Figure 6A, 6C). The Gli1 protein was significantly downregulated by B31 compared to compound **1** at 10 μM (Figure 6B, 6D). As expected, treatment with B31 significantly reduced the mRNA expression of Hh pathway target genes (Gli1 and Ptch1) in a dose-dependent manner (Figure 7A-D). Of note, the mRNA expression level of Gli1 and Ptch1 at 10 μM was markedly lower with B31 compared to compound **1**. This demonstrated that B31 prevented cell proliferation and promoted cell death as a consequence of suppressing the Hh signaling pathway.

Figure 6 should be here

Figure 6 Western blot analysis for Gli1 in PANC-1 and BxPC-3 cells treated with Vismodegib and B31.(A, C) Representative western blotting. (B, D) Densitometric analysis of the western blotting data. The results were calculated and expressed as a ratio of density of individual target proteins to the expression of β-actin. Data are shown as mean ± SD of three separate experiments (*P < 0.05, **P < 0.01, ***P < 0.001 vs. NC; $^{\#}$P < 0.05, $^{\#\#}$P < 0.01, $^{\#\#\#}$P < 0.001 vs. Vismodegib (10 μM), n = 3).

Figure 7 should be here

Figure 7 Real-time RT-qPCR analysis of Gli1 and Ptch1 in PANC-1 and BxPC-3 cells treated with Vismodegib and B31. GAPDH was used as an internal control.

mRNA expression levels are expressed as fold-change relative to the NC group. Data are shown as mean ± SD of three separate experiments (*P < 0.05, **P < 0.01, ***P < 0.001 vs. NC; $^{\#}$P < 0.05, $^{\#\#}$P < 0.01, $^{\#\#\#}$P < 0.001 vs. Vismodegib (10 μM), n = 3).

Given the involvement of the activated Hh signaling pathway in tumor metastasis, wound healing and transwell migration assays were performed. In Figure 8A and 8D, B31 significantly inhibited the migration ability of PANC-1 and BxPC-3 cells at 24 hours and 48 hours. The statistical results (Figures 8B-C and 8E-F) showed that the inhibition of cell migration increased in a concentration-dependent manner. Evidently, the wound closure and migration rate of B31 were lower compared to compound **1** at 10 μM.

Figure 8 should be here

Figure 8 Wound healing assay and transwell migration assay of PANC-1 and BxPC-3 cells treated with Vismodegib and B31. (A) Images acquired at the indicated time points. (B, C) Quantification of cell migration rates. (D) Photographs of the transwell migration assay. (E, F) Quantification of the percentages of cells at different concentrations. Data are shown as mean ± SD of three separate experiments. (*P < 0.05, **P < 0.01, vs. NC; $^{\#}$P < 0.05, vs. Vismodegib (10 μM), n = 3). Scale bar = 100 μm.

To examine the effect of B31 on apoptosis of pancreatic cancer cells, an Annexin V-PI double staining assay was performed. Compared with the control group, the proportion of apoptotic cells in the B31 group increased in a concentration-dependent manner (Figure 9). The apoptosis rates at 10 μM against PANC-1 and BxPC-3 cells were 28.14 ± 1.75 % and 24.71 ± 2.52 %, respectively, which were 3-fold higher than those of compound **1**. Additionally, the effect of B31 on cell cycle progression was investigated. The results showed that B31 arrested PANC-1 cells at the G2/M phase (Figures 10A and 10B) and BxPC-3 cells at the G0/G1 phase (Figures 10C and 10D).

Figure 9 should be here

Figure 9 Cell apoptosis analysis in PANC-1 and BxPC-3 cells treated with B31. (A, C) Analysis of apoptosis by flow cytometry. (B, D) Graphical representation of the total percentage of apoptosis induced by Vismodegib and B31 (*P < 0.05, **P < 0.01, ***P < 0.001 vs. NC; $^{\#}$P < 0.05, $^{\#\#}$P < 0.01, $^{\#\#\#}$P < 0.001 vs. Vismodegib (10 μM), n = 3).

Figure 10 should be here

Figure 10 Cell cycle analysis of PANC-1 and BxPC-3 cells treated with B31. (A,C) Representative histograms from flow cytometry. (B, D) Graphical representation of the percentage of cells in G0/G1, G2/M, and S-phases of the cell cycle (*P < 0.05,**P < 0.01 vs. NC, n = 3).

2.4 In vivo antitumor activity of B31

To evaluate the antitumor efficacy of B31 in vivo, a xenograft pancreatic cancer model was established using BxPC-3 cells. B31 and compound 1 were administered intraperitoneally daily based on body weight (Figure 11A).

Compared to the control group (Figure 11C-E), tumor growth was significantly inhibited in the tested groups. Tumor volumes in the compound **1** group (15 mg/kg) decreased by approximately 60%, while tumor volumes in the B31 group (5 mg/kg, 10 mg/kg, and 15 mg/kg) decreased by around 73%, 80%, and 82%, respectively. Consistently, tumor weight in the B31 group was lower compared to that in the compound **1** group at equal doses (Figure 11F). As expected, the groups treated with B31 exhibited notable suppression in pancreatic tumor growth, evidenced by the reduced levels of Gli1 protein detected via IHC (Figure 11G). Therefore, the potency of B31 was superior to that of compound **1** in treating pancreatic cancer tumors.

The potential toxic effect of B31 was investigated. The nude mice after diverse treatments showed no evident body weight drop (Figure 11B). The main organs (heart, liver, lungs, spleen and kidneys) of nude mice were harvested for H&E staining. As shown in Figure 12, there was no cellular edema, necrosis, inflammatory infiltration, or tissue fibrosis in the major organs of the tested groups, indicating that B31 had no toxic effects on the nude mice.

Figure 11 should be here

Figure 11 In vivo efficacy of Vismodegib and B31 in tumor-bearing nude mice. (A) Experimental design. (B) Body weight of animals during treatment. (C) Tumor size in various treatment groups. (D, E) Tumor volume. (F) Tumor weight. (G) Representative images of Gli1 IHC staining of tumor tissues. Data are expressed as the mean ± S.D. (*P < 0.05, **P < 0.01, ***P < 0.001 vs. NC; $^{\#}$P < 0.05, $^{\#\#}$P < 0.01 vs. Vismodegib (15 mg/kg), n = 6). Scale bar = 30 μm.

Figure 12 should be here

Figure 12 Analysis of major organs (heart, kidney, lung, liver and spleen) by H&E staining. Scale bar = 100 μm.

3.Conclusion

A series of novel Hh signaling pathway inhibitors with a pyridyl pyrimidine skeleton were explored through structural modification based on BMS-833923. The expanded SAR was described, and B31 was found to show the most potent Hh pathway inhibition, with an IC_{50} value of 2.7 nM. B31 was able to competitively bind to Smo protein, and molecular docking simulations indicated that it interacted with Smo via H-bonds, electrostatic force and hydrophobic force. In addition, B31 exhibited preferable antiproliferative effects against BxPC-3 and PANC-1 cells, as the expression of Gli1 proteins and the mRNA levels of Gli1 and Ptch1 were downregulated. Meanwhile, B31 weakened cell migration and promoted apoptosis. In the pancreatic cancer xenograft model, the B31 treatment group exhibited significant inhibition of tumor growth without any systemic toxicity. It is worth noting that tumor volumes in the high-dose group were reduced by 82%, which was 22% greater than that in the positive control

group. It is valuable to provide candidates for pyridyl pyrimidine Hh pathway inhibitors for targeted treatment of Hh-dependent PC.

4. Experimental Section

4.1 General

All chemicals were of analytical grade and purchased from commercial sources. All the organic reactions were checked by utilizing thin layer chromatography technique. Melting points were recorded on Melting Points SGWX-4B instrument (INESA, Shanghai, China). ^{1}H NMR and ^{13}C NMR spectra were measured on Bruker Avance 400 spectrometer (Bruker Biosciences, MA, USA). High-resolution mass spectra (HRMS) were determined on LCMS-IT-TOF spectrometer (SHIMADZU, Shanghai, China).

4.2 Synthesis

4.2.1 Procedure for the preparation of 3-(dimethylamino)-1-(pyridin-3-yl)prop-2-en-1-one (**5**)

Acetylpyridine (48.4 g, 0.4 mol) and N,N-dimethylformamide dimethylacetal (95.2 g, 0.8 mol) were dissolved in xylene (140 mL) and stirred mechanically at 140ºC for 20 hours. The methanol generated in the reaction was removed every 2 hours by distillation. The mixture was treated with n-hexane (40 mL) and stirred for another half an hour after cooling to room temperature. The precipitate was collected by filtration and washed with n-hexane. The crude product was purified by recrystallization in xylene to give the title compound (44.7 g, 63%) as light yellow crystals. m.p. 81-82 °C.

4.2.2 Procedure for the preparation of 4-(pyridin-3-yl)pyrimidin-2-amine (**6**)

Compound **5** (35.2 g, 0.2 mol), guanidine hydrochloride (19.1 g, 0.2mol), and sodium hydroxide (8 g, 0.2 mol) were dissolved in n-butanol (230 mL) and stirred mechanically at 120ºC for 12 hours. After cooling to room temperature, the precipitate was harvested by filtration and washed with cold dichloromethane. The filter cake was dried under vacuum to afford the title compound (23.7 g, 69%) as a white crystal.

4.2.3 Procedure for the preparation of methyl 4-((4-(pyridin-3-yl)pyrimidin-2-yl)amino)benzoate (**7**)

To a solution of compound 6 (8 g, 46 mmol) in dioxane (150 mL) were added methyl 4-bromobenzoate (11 g, 51 mmol), palladium acetate (1 g, 5 mmol), BINAP (5.8 g, 9 mmol), and cesium carbonate (30.3 g, 93 mmol). The mixture refluxed for 20 hours under N2 protection and was concentrated under vacuum. The residue was chromatographed on a silica gel column and eluted with a petroleum ether/ethyl acetate mixture (10:1 to 3:1, v/v) to give the title compound (12.4 g, 88%) as an orange powder. m.p. 187-189 °C. ^{1}H NMR (400 MHz, DMSO-*d6*) δ 10.25 (s, 1H), 9.37 (d, J = 1.8 Hz, 1H), 8.76 (dd, J = 4.7, 1.5 Hz, 1H), 8.69 (d, J = 5.2 Hz, 1H), 8.54 (dt, J = 8.0, 1.9 Hz, 1H), 8.02 – 7.94 (m, 4H), 7.61 (t, J = 5.4 Hz, 2H), 3.84 (s, 3H).

4.2.4 Procedure for the preparation of 4-((4-(pyridin-3-yl)pyrimidin-2-yl)amino)benzoic acid (**8**)

Compound **7** (12.4 g, 42 mmol) and sodium hydroxide (6.8 g, 170 mmol) were refluxed in an aqueous ethanol solution (250 mL) for 2 hours. The mixture was concentrated under vacuum and then diluted with 200 mL of water before being extracted with an equivalent volume of ethyl acetate. The water course was adjusted to

weakly acidic using dilute hydrochloric acid. The precipitate was collected by filtration and dried overnight. The title compound (11.8 g, 87%) was obtained as a yellow powder.

4.2.5 Procedure for the preparation of N-(pyridin-3-yl)-4-((4-(pyridin-3-yl)pyrimidin-2-yl)amino)benzamide (**9**)

Compound **8** (1 g, 3.4 mmol), HATU (1.3 g, 3.6 mmol), DIPEA (1.32 g, 10.2 mmol), and pyridin-3-amine (0.4 g, 4 mmol) were dissolved in N,N-Dimethylformamide (20 mL). The mixture was stirred at room temperature for 24 hours before being poured into water (100 mL). The precipitate was collected via filtration and dried for 6 hours. The title compound (0.7 g, 57%) as faint yellow powder was obtained. m.p. 230-232°C. ^{1}H NMR (400 MHz, DMSO-d_6) δ 10.31 (s, 1H), 10.19 (s, 1H), 9.40 (s, 1H), 8.98 (s, 1H), 8.77 (d, J = 3.2 Hz, 1H), 8.70 (d, J = 5.1 Hz, 1H), 8.55 (d, J = 8.0 Hz, 1H), 8.31 (dd, J = 4.6, 1.5 Hz, 1H), 8.23 (d, J = 8.6 Hz, 1H), 8.03 (s, 4H), 7.61 (d, J = 5.1 Hz, 2H), 7.40 (dd, J = 8.4, 4.7 Hz, 1H). ^{13}C NMR (100 MHz, DMSO-d_6) δ 165.93, 162.29, 160.40, 160.06, 152.18, 148.75, 144.77, 144.42, 142.46, 136.62, 134.99, 132.60, 129.21 (2C), 127.68, 127.13, 124.50, 124.00, 118.35 (2C), 109.61. HRMS(ESI) m/z calcd for $C_{21}H_{16}N_6O$ $[M+H]^+$ 369.1464, found 369.1446.

4.2.6 4-((4-(pyridin-3-yl)pyrimidin-2-yl)amino)-N-(3-(trifluoromethyl)phenyl)benzamide (**10**)

According to a procedure similar to that for compound 9, the faint yellow powder was obtained from compound **8** and 3-(trifluoromethyl)aniline with a yield of 62%. m.p. 179-181°C. ^{1}H NMR (400 MHz, DMSO-d_6) δ 10.41 (s, 1H), 10.19 (s, 1H), 9.40 (s, 1H), 8.77 (s, 1H), 8.71 (d, J = 5.1 Hz, 1H), 8.58 – 8.54 (m, 1H), 8.30 (s, 1H), 8.09 (d, J = 8.4 Hz, 1H), 8.03 (s, 4H), 7.61 (dd, J = 10.3, 6.6 Hz, 3H), 7.45 (d, J = 7.7 Hz, 1H). ^{13}C NMR (100 MHz, DMSO-d_6) δ 165.93, 162.31, 160.41, 160.08, 152.19, 148.76, 144.46, 140.79, 135.02, 132.63, 130.32, 130.01, 129.69, 129.22 (2C), 127.19, 124.53, 124.15, 120.12, 118.35 (2C), 116.72, 109.64. HRMS(ESI) m/z calcd for $C_{23}H_{16}F_3N_5O$ $[M+H]^+$ 436.1385, found 436.1366.

4.2.7 N-(3-fluorophenyl)-4-((4-(pyridin-3-yl)pyrimidin-2-yl)amino)benzamide (**11**)

According to a procedure similar to that for compound **9**, the faint yellow powder was obtained from compound **8** and 3-fluoroaniline, with a yield of 51%. m.p. 215-216 °C. ^{1}H NMR (400 MHz, DMSO-d_6) δ 10.32 (s, 1H), 10.23 (s, 1H), 9.43 (s, 1H), 8.80 (s, 1H), 8.73 (d, J = 5.2 Hz, 1H), 8.58 (d, J = 8.1 Hz, 1H), 8.15 – 8.01 (m, 3H), 7.83 (d, J = 11.9 Hz, 1H), 7.69 – 7.60 (m, 3H), 7.42 (q, J = 7.8 Hz, 1H), 6.96 (t, J = 8.5 Hz, 1H). ^{13}C NMR (100 MHz, DMSO-d_6) δ 165.82, 162.29, 161.42, 160.41, 160.05, 152.17, 148.75, 144.35, 141.84, 134.99, 132.60, 130.71, 129.17 (2C), 127.40, 124.49, 118.34 (2C), 116.37, 110.14, 109.60, 107.47. HRMS(ESI) m/z calcd for $C_{22}H_{16}FN_5O$ $[M+H]^+$ 386.1417, found 386.1402.

4.2.8 N-(3-fluoro-4-methylphenyl)-4-((4-(pyridin-3-yl)pyrimidin-2-yl)amino)benzamide (**12**)

According to a procedure similar to that for compound **9**, the faint yellow powder was obtained from compound **8** and 3-fluoro-4-methylaniline, with a yield of 65%. m.p. 233-234 °C. ^{1}H NMR (400 MHz, DMSO-d_6) δ 10.17 (d, J = 7.8 Hz, 2H), 9.39 (s, 1H), 8.77 (dd, J = 4.8, 1.6 Hz, 1H), 8.69 (d, J = 5.2 Hz, 1H), 8.55 (dt, J = 8.0, 2.0 Hz, 1H),

8.04 – 7.97 (m, 4H), 7.74 (dd, *J* = 12.5, 2.1 Hz, 1H), 7.62 (dd, *J* = 9.6, 5.0 Hz, 2H), 7.49 (dd, *J* = 8.3, 2.0 Hz, 1H), 7.24 (t, *J* = 8.6 Hz, 1H), 2.22 (s, 3H). ^{13}C NMR (100 MHz, DMSO-*d*$_6$) δ 165.60, 162.28, 160.41, 160.04, 159.53, 152.17, 148.75, 144.24, 139.42, 134.98, 132.61, 131.74, 129.09 (2C), 127.51, 124.49, 119.10, 118.34 (2C), 116.20, 109.56, 107.40, 14.22. HRMS(ESI) m/z calcd for $C_{23}H_{18}FN_5O$ $[M+H]^+$ 400.1574, found 400.1577.

4.2.9 N-(3-fluoro-4-morpholinophenyl)-4-((4-(pyridin-3-yl)pyrimidin-2-yl)amino)benzamide (**13**)

According to a procedure similar to that for compound **9**, the faint yellow powder was obtained from compound **8** and 3-fluoro-4-morpholinoaniline, with a yield of 49%. m.p. 265-267°C. ^{1}H NMR (400 MHz, DMSO-*d*$_6$) δ 10.14 (d, *J* = 12.9 Hz, 2H), 9.40 (s, 1H), 8.77 (d, *J* = 4.8 Hz, 1H), 8.70 (d, *J* = 5.1 Hz, 1H), 8.55 (d, *J* = 8.0 Hz, 1H), 8.01 (t, *J* = 7.4 Hz, 4H), 7.75 (d, *J* = 15.2 Hz, 1H), 7.62 (t, *J* = 6.9 Hz, 2H), 7.51 (d, *J* = 8.1 Hz, 1H), 7.05 (t, *J* = 9.3 Hz, 1H), 3.76 (s, 4H), 2.99 (s, 4H). ^{13}C NMR (100 MHz, DMSO-*d*$_6$) δ 165.36, 162.28, 160.42, 160.06, 156.09, 153.68, 152.18, 148.75, 144.17, 135.84, 134.99, 132.61, 129.02 (2C), 127.57, 124.50, 119.46, 118.34 (2C), 116.70, 109.55, 109.03, 66.73 (2C), 51.32 (2C). HRMS(ESI) m/z calcd for $C_{26}H_{23}FN_6O_2$ $[M+H]^+$ 471.1945, found 471.1927.

4.2.10 N-(3-fluoro-5-methylphenyl)-4-((4-(pyridin-3-yl)pyrimidin-2-yl)amino)benzamide (**14**)

According to a procedure similar to that for compound **9**, the faint yellow powder was obtained from compound **8** and 3-fluoro-5-methylaniline, with a yield of 46%. m.p. 226-228°C. ^{1}H NMR (400 MHz, DMSO-*d*$_6$) δ 10.15 (s, 2H), 9.38 (s, 1H), 8.71 (dd, *J* = 30.7, 5.3 Hz, 2H), 8.52 (s, 1H), 7.99 (s, 4H), 7.59 (d, *J* = 5.6 Hz, 3H), 7.42 (s, 1H), 6.73 (d, *J* = 9.5 Hz, 1H), 2.31 (s, 3H). ^{13}C NMR (100 MHz, DMSO-*d*$_6$) δ 165.74, 162.28, 161.37, 160.40, 160.02, 152.15, 148.75, 144.31, 141.32, 140.62, 134.97, 132.60, 129.13 (2C), 127.45, 124.47, 118.33 (2C), 116.86, 110.76, 109.56, 104.70, 21.67. HRMS(ESI) m/z calcd for $C_{23}H_{18}FN_5O$ $[M+H]^+$ 400.1574, found 400.1555.

4.2.11 N-(3-methylphenyl)-4-((4-(pyridin-3-yl)pyrimidin-2-yl)amino)benzamide (**15**)

According to a procedure similar to that for compound **9**, the faint yellow powder was obtained from compound **8** and m-toluidine, with a yield of 64%. m.p. 205-206 °C. ^{1}H NMR (400 MHz, DMSO-*d*$_6$) δ 10.14 (s, 1H), 10.00 (s, 1H), 9.39 (d, *J* = 2.3 Hz, 1H), 8.76 (dd, *J* = 4.8, 1.6 Hz, 1H), 8.69 (d, *J* = 5.2 Hz, 1H), 8.54 (dt, *J* = 8.1, 2.0 Hz, 1H), 7.99 (s, 4H), 7.67 – 7.55 (m, 4H), 7.23 (t, *J* = 7.8 Hz, 1H), 6.91 (d, *J* = 7.5 Hz, 1H), 2.32 (s, 3H). ^{13}C NMR (100 MHz, DMSO-*d*$_6$) δ 165.50, 162.27, 160.44, 160.01, 152.14, 148.75, 144.08, 139.89, 138.18, 134.97, 132.62, 129.05 (2C), 128.90, 127.89, 124.57, 124.47, 121.37, 118.35 (2C), 118.01, 109.50, 21.75. HRMS(ESI) m/z calcd for $C_{23}H_{19}N_5O$ $[M+H]^+$ 382.1668, found 382.1650.

4.2.12 N-(2-methylphenyl)-4-((4-(pyridin-3-yl)pyrimidin-2-yl)amino)benzamide (**16**)

According to a procedure similar to that for compound **9**, the faint yellow powder was obtained from compound **8** and o-toluidine, with a yield of 67%. m.p. 204-205 °C. ^{1}H NMR (400 MHz, DMSO-*d*$_6$) δ 10.13 (s, 1H), 9.71 (s, 1H), 9.39 (s, 1H), 8.76 (dd, *J*

= 4.8, 1.6 Hz, 1H), 8.69 (d, *J* = 5.2 Hz, 1H), 8.54 (dt, *J* = 8.0, 2.0 Hz, 1H), 8.00 (s, 4H), 7.61 (dd, *J* = 9.8, 5.0 Hz, 2H), 7.36 (d, *J* = 6.5 Hz, 1H), 7.30 – 7.12 (m, 3H), 2.25 (s, 3H). ^{13}C NMR (100 MHz, DMSO-d_6) δ 165.37, 162.29, 160.45, 160.01, 152.15, 148.75, 144.05, 137.24, 134.98, 134.14, 132.62, 130.78, 129.03 (2C), 127.53, 127.08, 126.46, 126.25, 124.48, 118.41 (2C), 109.50, 18.48. HRMS(ESI) m/z calcd for $C_{23}H_{19}N_5O$ $[M+H]^+$ 382.1668, found 382.1651.

4.2.13 N-(2-methoxyphenyl)-4-((4-(pyridin-3-yl)pyrimidin-2-yl)amino)benzamide (**17**)

According to a procedure similar to that for compound **9**, the faint yellow powder was obtained from compound **8** and 2-methoxyaniline, with a yield of 71%. m.p. 184-185 °C. ^{1}H NMR (400 MHz, DMSO-d_6) δ 10.15 (s, 1H), 9.38 (s, 1H), 9.24 (s, 1H), 8.76 (dd, *J* = 4.8, 1.7 Hz, 1H), 8.69 (d, *J* = 5.1 Hz, 1H), 8.55 (dt, *J* = 8.1, 2.0 Hz, 1H), 8.04 – 7.94 (m, 4H), 7.85 (dd, *J* = 7.9, 1.6 Hz, 1H), 7.62 (dd, *J* = 9.7, 5.0 Hz, 2H), 7.16 (td, *J* = 7.8, 7.3, 1.7 Hz, 1H), 7.10 (dd, *J* = 8.3, 1.5 Hz, 1H), 6.97 (td, *J* = 7.6, 1.4 Hz, 1H), 3.86 (s, 3H). ^{13}C NMR (100 MHz, DMSO-d_6) δ 164.97, 162.32, 160.43, 159.98, 152.14, 151.54, 148.76, 144.19, 134.99, 132.61, 128.84 (2C), 127.72, 127.42, 125.70, 124.49, 124.14, 120.75, 118.47 (2C), 111.76, 109.55, 56.25. HRMS(ESI) m/z calcd for $C_{23}H_{19}N_5O_2$ $[M+H]^+$ 398.1617, found 398.1599.

4.2.14 N-(4-methoxyphenyl)-4-((4-(pyridin-3-yl)pyrimidin-2-yl)amino)benzamide (**18**)

According to a procedure similar to that for compound **9**, the faint yellow powder was obtained from compound **8** and 4-methoxyaniline, with a yield of 63%. m.p. 240-241 °C. ^{1}H NMR (400 MHz, DMSO-d_6) δ 10.12 (s, 1H), 9.96 (s, 1H), 9.38 (d, *J* = 2.3 Hz, 1H), 8.76 (dd, *J* = 4.8, 1.6 Hz, 1H), 8.68 (d, *J* = 5.1 Hz, 1H), 8.54 (dt, *J* = 8.1, 2.0 Hz, 1H), 7.98 (d, *J* = 1.8 Hz, 4H), 7.73 – 7.65 (m, 2H), 7.65 – 7.57 (m, 2H), 6.97 – 6.88 (m, 2H), 3.75 (s, 3H). ^{13}C NMR (100 MHz, DMSO-d_6) δ 165.17, 162.26, 160.44, 160.00, 155.89, 152.14, 148.74, 143.94, 134.96, 133.03, 132.62, 128.93 (2C), 127.96, 124.46, 122.43 (2C), 118.35 (2C), 114.22 (2C), 109.47, 55.67. HRMS(ESI) m/z calcd for $C_{23}H_{19}N_5O_2$ $[M+H]^+$ 398.1617, found 398.1599.

4.2.15 N-(3,4-dimethoxyphenyl)-4-((4-(pyridin-3-yl)pyrimidin-2-yl)amino)benzamide (**19**)

According to a procedure similar to that for compound **9**, the faint yellow powder was obtained from compound **8** and 3,4-dimethoxyaniline, with a yield of 75%. m.p. 227-228 °C. ^{1}H NMR (400 MHz, DMSO-d_6) δ 10.13 (s, 1H), 9.94 (s, 1H), 9.39 (d, *J* = 2.2 Hz, 1H), 8.76 (dd, *J* = 4.8, 1.6 Hz, 1H), 8.69 (d, *J* = 5.1 Hz, 1H), 8.54 (dt, *J* = 8.0, 2.0 Hz, 1H), 7.99 (s, 4H), 7.61 (dd, *J* = 10.3, 5.0 Hz, 2H), 7.50 (d, *J* = 2.4 Hz, 1H), 7.35 (dd, *J* = 8.7, 2.4 Hz, 1H), 6.93 (d, *J* = 8.7 Hz, 1H), 3.76 (d, *J* = 8.2 Hz, 6H). ^{13}C NMR (100 MHz, DMSO-d_6) δ 165.16, 162.27, 160.44, 160.01, 152.14, 148.96, 148.74, 145.48, 143.97, 134.96, 133.55, 132.62, 128.91 (2C), 127.95, 124.46, 118.34 (2C), 112.74, 112.44, 109.48, 106.02, 56.24, 55.90. HRMS(ESI) m/z calcd for $C_{24}H_{21}N_5O_3$ $[M+H]^+$ 428.1723, found 428.1705.

4.2.16 N-(3,5-dimethoxyphenyl)-4-((4-(pyridin-3-yl)pyrimidin-2-yl)amino)benzamide (**20**)

According to a procedure similar to that for compound **9**, the faint yellow powder was obtained from compound **8** and 3,5-dimethoxyaniline, with a yield of 69%. m.p. 193-195°C. ^{1}H NMR (400 MHz, DMSO-d_6) δ 10.16 (s, 1H), 10.01 (s, 1H), 9.40 (d, *J* = 2.3 Hz, 1H), 8.77 (dd, *J* = 4.9, 1.6 Hz, 1H), 8.70 (d, *J* = 5.1 Hz, 1H), 8.56 (d, *J* = 8.1 Hz, 1H), 8.00 (d, *J* = 4.6 Hz, 4H), 7.63 (dd, *J* = 8.8, 4.9 Hz, 2H), 7.13 (d, *J* = 2.3 Hz, 2H), 6.26 (s, 1H), 3.76 (s, 6H). ^{13}C NMR (100 MHz, DMSO-d_6) δ 165.58, 162.29, 160.89 (2C), 160.42, 160.06, 152.18, 148.75, 144.16, 141.66, 134.99, 132.62, 129.06 (2C), 127.75, 124.51, 118.31 (2C), 109.56, 98.92, 95.98, 55.60 (2C). HRMS(ESI) m/z calcd for $C_{24}H_{21}N_5O_3$ $[M+H]^+$ 428.1723, found 428.1727.

4.2.17 N-(3,4,5-trimethoxyphenyl)-4-((4-(pyridin-3-yl)pyrimidin-2-yl)amino)benzamide (**21**)

According to a procedure similar to that for compound **9**, the faint yellow powder was obtained from compound **8** and 3,4,5-trimethoxyaniline, with a yield of 81%. m.p. 232-233 °C. ^{1}H NMR (400 MHz, DMSO-d_6) δ 10.14 (s, 1H), 9.98 (s, 1H), 9.39 (s, 1H), 8.76 (dd, *J* = 4.8, 1.6 Hz, 1H), 8.69 (d, *J* = 5.1 Hz, 1H), 8.54 (dt, *J* = 8.1, 2.0 Hz, 1H), 8.04 – 7.94 (m, 4H), 7.62 (dd, *J* = 8.5, 4.9 Hz, 2H), 7.26 (s, 2H), 3.78 (s, 6H), 3.65 (s, 3H). ^{13}C NMR (100 MHz, DMSO-d_6) δ 165.33, 162.28, 160.43, 160.04, 153.11 (2C), 152.17, 148.75, 144.11, 136.11, 134.97, 134.01, 132.62, 128.95 (2C), 127.76, 124.49, 118.33 (2C), 109.54, 98.45 (2C), 60.63, 56.23 (2C). HRMS(ESI) m/z calcd for $C_{25}H_{23}N_5O_4$ $[M+H]^+$ 458.1828, found 458.1810.

4.2.18 N-(4-ethoxyphenyl)-4-((4-(pyridin-3-yl)pyrimidin-2-yl)amino)benzamide (**22**)

According to a procedure similar to that for compound **9**, the faint yellow powder was obtained from compound **8** and 4-ethoxyaniline, with a yield of 67%. m.p. 249-250 °C. ^{1}H NMR (400 MHz, DMSO-d_6) δ 10.09 (s, 1H), 9.96 (s, 1H), 9.32 (s, 1H), 8.69 (d, *J* = 3.2 Hz, 1H), 8.61 (d, *J* = 5.2 Hz, 1H), 8.47 (d, *J* = 8.1 Hz, 1H), 7.93 (s, 4H), 7.63 (d, *J* = 8.7 Hz, 2H), 7.56-7.52 (m, 2H), 6.84 (d, *J* = 8.9 Hz, 2H), 3.94 (q, *J* = 7.0 Hz, 2H), 1.26 (t, *J* = 6.9 Hz, 3H). ^{13}C NMR (100 MHz, DMSO-d_6) δ 165.15, 162.26, 160.45, 160.03, 155.12, 152.16, 148.74, 143.93, 134.98, 132.97, 132.62, 128.98 (2C), 127.94, 124.49, 122.45 (2C), 118.32 (2C), 114.71 (2C), 109.48, 63.59, 15.23. HRMS(ESI) m/z calcd for $C_{24}H_{21}N_5O_2$ $[M+H]^+$ 412.1773, found 412.1771.

4.2.19 N-(4-morpholinophenyl)-4-((4-(pyridin-3-yl)pyrimidin-2-yl)amino)benzamide (**23**)

According to a procedure similar to that for compound **9**, the faint yellow powder was obtained from compound **8** and 4-morpholinoaniline, with a yield of 52%. m.p. 285-287 °C. ^{1}H NMR (400 MHz, DMSO-d_6) δ 10.13 (s, 1H), 9.92 (s, 1H), 9.40 (s, 1H), 8.77 (dd, *J* = 4.8, 1.6 Hz, 1H), 8.70 (d, *J* = 5.2 Hz, 1H), 8.56 (dt, *J* = 8.1, 2.0 Hz, 1H), 7.99 (d, *J* = 1.7 Hz, 4H), 7.68 – 7.60 (m, 4H), 6.95 (d, *J* = 9.1 Hz, 2H), 3.80 – 3.72 (m, 4H), 3.13 – 3.06 (m, 4H). ^{13}C NMR (100 MHz, DMSO-d_6) δ 165.03, 162.28, 160.45, 160.06, 152.18, 148.75, 147.86, 143.86, 134.99, 132.63, 132.16, 128.89 (2C), 128.06, 124.51, 121.94 (2C), 118.33 (2C), 115.79 (2C), 109.48, 66.65 (2C), 49.45 (2C). HRMS(ESI) m/z calcd for $C_{26}H_{24}N_6O_2$ $[M+H]^+$ 453.2039, found 453.2042.

4.2.20 N-(4-(4-methylpiperazin-1-yl)phenyl)-4-((4-(pyridin-3-yl)pyrimidin-2-yl)amino) benzamide (**24**)

According to a procedure similar to that for compound **9**, the faint yellow powder was obtained from compound **8** and 4-(4-methylpiperazin-1-yl)aniline, with a yield of 47%. m.p. 271-273°C. ^{1}H NMR (400 MHz, DMSO-d_6) δ 10.13 (s, 1H), 9.91 (s, 1H), 9.40 (s, 1H), 8.73 (d, *J* = 31.3 Hz, 2H), 8.55 (s, 1H), 7.99 (s, 4H), 7.73 – 7.55 (m, 4H), 7.13 – 6.68 (m, 2H), 3.11 (s, 4H), 2.47 (s, 4H), 2.23 (s, 3H). ^{13}C NMR (100 MHz, DMSO-d_6) δ 164.99, 162.27, 160.45, 160.05, 152.17, 148.75, 147.86, 143.84, 134.98, 132.63, 131.82, 128.88 (2C), 128.08, 124.50, 121.94 (2C), 118.33 (2C), 116.01 (2C), 109.47, 55.18 (2C), 49.06 (2C), 46.30. HRMS(ESI) m/z calcd for $C_{27}H_{27}N_7O$ $[M+H]^+$ 466.2355, found 466.2335.

4.2.21 N-(4-((dimethylamino)methyl)phenyl)-4-((4-(pyridin-3-yl)pyrimidin-2-yl)amino) benzamide (**25**)

According to a procedure similar to that for compound **9**, the faint yellow powder was obtained from compound **8** and 4-((dimethylamino)methyl)aniline, with a yield of 60%. m.p. 218-220°C. ^{1}H NMR (400 MHz, DMSO-d_6) δ 10.15 (s, 1H), 10.04 (s, 1H), 9.40 (s, 1H), 8.77 (dd, *J* = 4.8, 1.6 Hz, 1H), 8.70 (d, *J* = 5.1 Hz, 1H), 8.55 (d, *J* = 8.1 Hz, 1H), 8.01 (m, 4H), 7.76 (d, *J* = 8.4 Hz, 1H), 7.64-7.61 (m, 2H), 7.26 (d, *J* = 8.3 Hz, 2H), 3.37 (s, 2H), 2.16 (s, 6H). ^{13}C NMR (100 MHz, DMSO-d_6) δ 165.46, 162.28, 160.44, 160.04, 152.17, 148.75, 144.07, 138.74, 134.99, 134.26, 132.62, 129.47 (2C), 129.04 (2C), 127.87, 124.50, 120.56 (2C), 118.34 (2C), 109.52, 63.50, 45.37 (2C). HRMS(ESI) m/z calcd for $C_{25}H_{24}N_6O$ $[M+H]^+$ 425.2090, found 425.2071.

4.2.22 N-(4-trifluoromethoxyphenyl)-4-((4-(pyridin-3-yl)pyrimidin-2-yl)amino)benzamide (**26**)

According to a procedure similar to that for compound **9**, the faint yellow powder was obtained from compound **8** and 4-trifluoromethoxyaniline, with a yield of 64%. m.p. 245-246 °C. ^{1}H NMR (400 MHz, DMSO-d_6) δ 10.28 (s, 1H), 10.17 (s, 1H), 9.40 (s, 1H), 8.77 (d, *J* = 4.8 Hz, 1H), 8.70 (d, *J* = 5.2 Hz, 1H), 8.56 (d, *J* = 8.0 Hz, 1H), 8.04 – 7.99 (m, 4H), 7.93 (d, *J* = 9.0 Hz, 2H), 7.67 – 7.59 (m, 2H), 7.38 (d, *J* = 8.6 Hz, 2H). ^{13}C NMR (100 MHz, DMSO-d_6) δ 165.70, 162.30, 160.42, 160.06, 152.18, 148.77, 144.32, 144.17, 139.21, 134.99, 132.61, 129.16 (2C), 127.42, 124.50, 122.04 (2C), 121.94 (2C), 119.47, 118.34 (2C), 109.59. HRMS(ESI) m/z calcd for $C_{23}H_{16}F_3N_5O_2$ $[M+H]^+$ 452.1334, found 452.1334.

4.2.23 N-(4-fluorophenyl)-4-((4-(pyridin-3-yl)pyrimidin-2-yl)amino)benzamide (**27**)

According to a procedure similar to that for compound **9**, the faint yellow powder was obtained from compound **8** and 4-fluoro aniline, with a yield of 52%. m.p. 245-247 °C. ^{1}H NMR (400 MHz, DMSO-d_6) δ 10.16 (s, 2H), 9.40 (s, 1H), 8.73 (dd, *J* = 30.3, 4.9 Hz, 2H), 8.55 (d, *J* = 8.0 Hz, 1H), 8.01 (s, 4H), 7.83 (dd, *J* = 8.7, 5.0 Hz, 2H), 7.61 (d, *J* = 4.8 Hz, 2H), 7.20 (t, *J* = 8.7 Hz, 2H). ^{13}C NMR (100 MHz, DMSO-d_6) δ 165.49, 162.28, 160.42, 160.03, 159.85, 152.16, 148.75, 144.16, 136.33, 134.98, 132.61, 129.05 (2C), 127.63, 124.48, 122.53 (2C), 118.35 (2C), 115.73 (2C), 109.54. HRMS(ESI) m/z calcd for $C_{22}H_{16}FN_5O$ $[M+H]^+$ 386.1417, found 386.1399.

4.2.24 N-(4-chlorophenyl)-4-((4-(pyridin-3-yl)pyrimidin-2-yl)amino)benzamide (**28**)

According to a procedure similar to that for compound **9**, the faint yellow powder was obtained from compound **8** and 4-chloro aniline, with a yield of 56%. m.p. 260-262 °C. ^{1}H NMR (400 MHz, DMSO-d_6) δ 10.22 (s, 1H), 10.17 (s, 1H), 9.39 (s, 1H), 8.77 (dd, J = 4.8, 1.7 Hz, 1H), 8.70 (d, J = 5.2 Hz, 1H), 8.57 – 8.53 (m, 1H), 8.04 – 7.98 (m, 4H), 7.85 (d, J = 8.9 Hz, 2H), 7.62 (d, J = 5.1 Hz, 2H), 7.42 (d, J = 8.9 Hz, 2H). ^{13}C NMR (100 MHz, DMSO-d_6) δ 165.65, 162.29, 160.41, 160.04, 152.17, 148.75, 144.27, 138.96, 134.99, 132.61, 130.86, 129.13 (2C), 128.98 (2C), 127.50, 124.49, 122.25 (2C), 118.34 (2C), 109.57. HRMS(ESI) m/z calcd for $C_{22}H_{16}ClN_5O$ $[M+H]^+$ 402.1122, found 402.1105.

4.3 Gli Luciferase reporter assay

The NIH3T3 cells, which involve Gli-dependent dual-luciferase, were cultured in DMEM containing calf serum, penicillin, streptomycin, and glutamine. The cells were then seeded in 96-well plates and incubated overnight, followed by various treatments for 48 hours as indicated. The luciferase activity in the cell lysates was measured using a dual-luciferase reporter assay system (Promega) according to the manufacturer's instructions in a luminometer (GloMax 20/20, Promega, USA). The firefly luciferase values were normalized to renilla values.

4.4 Fluorescence binding assays

The Smo (GenePharma, China) plasmid was stably transfected into HEK-297T cells, and its transfection efficiency was confirmed via Western blot analysis. Subsequently, 100 μL of 100 μg/mL poly-L-lysine solution was added to each well of a 96-well plate and incubated in a cell culture incubator for 2 hours before removal. Following this, 2×10^4 cells were seeded into each well and cultured for 24 hours. Afterward, the cells were fixed and stained with 4% paraformaldehyde and DAPI. Then, BODIPY-Cyclopamine (100 nM) (Biovision, USA) and the test compounds B31 and Vismodegib (Bidepharm, China) were added to each well, and the plate was incubated for 2 hours. After incubation, the signal intensity of green fluorescence in the cells was detected using a fluorescence microscope (Axio Observer, Carl Zeiss, Oberkochen, Germany).

4.5 Molecular modeling study

The protein co-crystallized with vismodegib was downloaded from the PDB database (PDB code: 5L7I). Subunit B of the crystal was used to prepare a docking model before its optimization, which included amino acid protonation, removal of crystal water and the original ligand, and definition of the loop region. The optimal conformation of B31 was output when its CHARMM force field parameters were under minimization. B31 was located at the center of original ligand, and its docking radius was 10 Å. The docking result was recorded using AutoDock Vina 1.1.2. Ultimately, the interaction between B31 and the protein was analyzed using Discovery Studio 4.5.

4.6 Cells and cell culture

The PANC-1 and BxPC-3 cell lines were obtained from Wuhan Procell Life Science & Technology Co., Ltd. The cells were passaged in DMEM and RPMI 1640 (Coring, USA) containing 10% FBS (Evergreen, China), penicillin (100 U/mL), and streptomycin (100 μg/mL). Incubation was done in a humidified incubator controlled at 5% CO_2 and 37°C. Cell passaging was performed every 2 days.

4.7 Cell proliferation assay

PANC-1 and BxPC-3 cells in the logarithmic growth phase were prepared as a cell suspension and seeded into a 96-well plate at a density of 8,000-10,000 cells per well, with a total volume of 100 μL. Six wells were used as blank controls, containing only culture medium. The plate was then incubated overnight at 37° C with 5% CO_2 to allow for cell adhesion. Vismodegib or B31 was dissolved in DMSO and diluted to the specified concentrations in the culture medium. The next day, the supernatant was removed, and 100 μL of culture medium containing different drug concentrations was added to each well, with the negative control receiving drug-free medium. The plate was incubated for an additional 48 hours. Carefully, the supernatant was aspirated, and 90 μL of fresh culture medium was added, followed by the addition of 10 μL of MTT solution (5 mg/mL). The plate was then further incubated at 37° C for 4 hours. After aspirating the supernatant, 100 μL of DMSO was added to each well, and the plate was placed on a shaker in the dark at low-speed for 10 minutes to ensure complete dissolution of the crystals. The absorbance values of each well were measured using an ELISA reader (Moleculai Devices, USA) at a wavelength of 490 nm. Cell viability was calculated as [(treatment group - blank group) / (negative control group - blank group)] × 100%. The IC_{50} value was determined by fitting a curve.

4.8 Western blot analysis

After seeding PANC-1 and BxPC-3 cells into 6-well plates, they were treated with different concentrations of Vismodegib and B31 for 48 hours. Subsequently, the cells were lysed in RIPA buffer containing a 1:100 dilution of PMSF (Beyotime, Shanghai, China). Cells were scraped off the plates and collected into 1.5 mL EP tubes, followed by cell lysis using a cell sonicator. The lysates were then centrifuged at 14,000 rpm for 10 minutes at 4° C, and the supernatants were collected into new 1.5 mL EP tubes as total protein samples. Protein concentration was determined using the BCA Protein Assay Kit (Beyotime Biotechnology, Shanghai, China) according to the manufacturer's instructions. Total protein samples were adjusted to 20-30 μg, boiled in a water bath for 5 minutes to denature, and then cooled and stored at -20° C.

SDS-PAGE gels were prepared according to the instructions provided with the SDS-PAGE Gel Preparation Kit (Beyotime Biotechnology, Shanghai, China). Protein samples were then separated by 6-12% gradient SDS-PAGE electrophoresis and transferred onto PVDF membranes (Millipore, Shanghai, China). The membranes were blocked with 5% skim milk or BSA blocking solution on a shaker at room temperature for 2 hours, followed by incubation with primary antibodies against Gli1 (CST, USA) overnight at 4° C. The next day, the membranes were washed three times with TBST on a shaker and then incubated with corresponding secondary antibodies (Beyotime Biotechnology, Shanghai, China) at room temperature for 1.5 hours. After washing with TBST, signal development was achieved using the BeyoECL Plus Chemiluminescence Kit (Beyotime Biotechnology, Shanghai, China). Band images were visualized using an ECL imaging system. Subsequently, the bands were analyzed using ImageJ software, and the results were calculated. β-actin was used as an internal control for the analysis.

4.9 qRT-PCR analysis

For quantitative real-time RT-PCR analysis, RNA was extracted from PANC-1 and BxPC-3 cells treated with different concentrations of Vismodegib and B31 for 48 hours using the RNeasy Mini Kit (QIAGEN, MD). The RNA concentration was measured using a NanoDrop 2000 spectrophotometer (Thermo Fisher Scientific, USA), and the OD values were recorded (OD values between 1.8-2.0 indicate high RNA concentration). Subsequently, RNA was reverse transcribed into cDNA using a reverse transcription kit (Vazyme, China) on a thermocycler (Thermo Fisher Scientific, USA). Primers were synthesized by Takara and had the following sequences: Gli1-Forward primer: ATCCTTACCTCCCAACCTCTGT, Reverse primer: AACTTCTGGCTCTTCCTGTAGC; Ptch1-Forward primer: CTCCTTTGCGGTGGACAA, Reverse primer: CCTCAGCCTTATTCAGCATTTC; GAPDH-Forward primer: AGAAGGCTGGGGCTCATTTG, Reverse primer: AGGGGCCATCCACAGTCTTC. Subsequently, the ChamQ Universal SYBR qPCR Master Mix (Vazyme, China) was used to prepare the reaction mixture, and real-time RT-PCR amplification of cDNA was performed on a 7500 qPCR system (ABI, USA).

4.10 Wound healing assay

The PANC-1 and BxPC-3 cells, in logarithmic growth phase, were evenly distributed into a 6-well plate and incubated overnight in a cell culture incubator. When the cell confluence reached 80-90% in the wells, a "cross" was scratched in each well using a pipette gun with a 20-200 μL tip. The supernatant was discarded, and the cells were gently washed three times with PBS. During the third wash, photographs were taken under a microscope, with 8 fields selected and recorded as 0 h. After discarding the PBS, 2 mL of pre-prepared medium containing 2% FBS and different concentrations of Vismodegib and B31 was added to each well, and the plate was returned to the incubator for further incubation. After 24 hours, photographs were taken of the fields that were photographed at 0 h (100× magnification). The percentage of scratch closure was calculated as follows: Percentage of scratch closure % = [(scratch area at 0 h - scratch area at 24 h) / scratch area at 0 h] × 100%.

4.11 Transwell migration assays

The migration ability of PANC-1 and BxPC-3 cells was assessed using Transwell chamber inserts (Costar, New York, USA). Cells in logarithmic growth phase were digested and centrifuged to prepare single-cell suspensions for cell counting. Based on the cell count, cell suspensions were prepared in serum-free medium at a concentration of 1.5×10^5 cells/mL with varying concentrations of drugs. Subsequently, 800 μL of medium containing 10% FBS was added to the lower chamber, while 200 μL of cell suspension containing different concentrations of Vismodegib and B31 was added dropwise to the upper chamber. After 48 hours of incubation in a cell culture incubator, the medium in the upper chamber was aspirated, and the cells in the upper chamber were gently wiped with a cotton swab. A new 24-well plate was then fixed with 4% paraformaldehyde, and the inserts were placed in the wells for fixation. After 15-20 minutes, the inserts were transferred to wells containing approximately 800 μL of 0.5% crystal violet solution (Solarbio, China) for staining. After staining, excess dye on the upper surface of the inserts was gently wiped off with a cotton swab. Subsequently, the

inserts were observed and photographed under a microscope (100× magnification), and four random fields were selected for imaging and cell counting.

4.12 Cell apoptosis and cycle assay

Pancreatic cancer cells PANC-1 and BxPC-3 (1.0×10^6 cells/well, 6-well plate) were treated with varying concentrations of B31 for 48 hours. The supernatant was collected into 10 mL centrifuge tubes, and the cells were washed with PBS, digested, and collected into the aforementioned 10 mL centrifuge tubes. Centrifugation was done at 1000 rpm for 3 minutes, and the supernatant was discarded. Subsequently, pre-prepared 1× Annexin V Binding Solution was added to achieve a final cell suspension concentration of 1×10^6 cells/mL.

For apoptosis analysis, 100 μL of the prepared cell suspension was transferred to a 1.5 mL light-protected centrifuge tube, and 5 μL of Annexin V FITC conjugate and 5 μL of PI Solution were added to the sample tube (control tubes were set up: unstained cells, Annexin V FITC stained cells, PI stained cells). The tubes were then incubated in the dark at room temperature for 15 minutes, followed by the addition of 400 μL of 1× Annexin V Binding Solution.

For cell cycle analysis, the prepared cell suspension was transferred to a 1.5 mL light-protected EP tube, and 500 μL of 70% pre-cooled ethanol was added for overnight fixation at 4° C. The next day, the fixation solution was discarded, and the cells were washed with PBS, followed by centrifugation. The cell pellet was resuspended in 100 μL of RNase A solution and incubated at 37° C for 30 minutes, then 400 μL of PI staining solution was added and mixed well. The cells were incubated in the dark at 4° C for 30 minutes. Apoptosis and cell cycle distribution were measured within 1 hour using the BD Accuri C6 Plus flow cytometer (BD Biosciences, Beijing, China).

4.13 In vivo anti-tumor effects in BxPC nude mice xenograft model

30 female BALB/c nude mice (5 weeks old, weighing 16 ± 2 g) were purchased from Beijing Huafukang Biotechnology Co., Ltd. (China) and housed in the SPF-grade animal facility at the Animal Experimental Center of Shenyang Medical College. They were provided with ad libitum access to water and food.

Sufficient pancreatic cancer cells BxPC-3 were cultured in advance, harvested, and adjusted to a concentration of 5×10^6 cells/mL with serum-free medium. A volume of 200 μL of cell suspension was subcutaneously injected into the right axilla of each nude mice. Flattened or round tumors appeared 7-10 days after injection, indicating successful inoculation, with only one tumor observed per animal.

Tumors were measured daily with a caliper. When the tumor volume reached 100 mm^3, the nude mice were randomly divided into six groups (n=6/group): saline control group, Vismodegib group, low-dose B31 group, medium-dose B31 group, and high-dose B31 group, with Vismodegib serving as the positive control to evaluate the efficacy of B31. The formula used to calculate tumor volume was: Volume = $(a\times b^2)/2$, where 'a' represents length and 'b' represents width. Treatment lasted for 21 days, with daily measurements of mouse body weight and tumor size taken every other day. Upon completion of treatment, the nude mice were euthanized by cervical dislocation the following day. Tumors and the five major organs (heart, liver, lung, spleen, and kidney) were dissected, washed with sterile saline, dried with filter paper, and photographed.

Tumor size was measured with a caliper, and tumor weight was measured using an analytical balance. Tumors and organs were then fixed in 4% paraformaldehyde.

4.14 H&E staining

The five major organs of nude mice were fixed in 4% paraformaldehyde for 3-7 days, followed by paraffin embedding and sectioning (4 μm thickness). The tissue-containing slides were placed in a slide oven at 60° C for approximately 1 hour for dewaxing. Dewaxing was performed twice in xylene for 10 minutes each, followed by a series of ethanol gradients (100%, 95%, 85%, 75%) for 5 minutes each, soaking in distilled water for 5 minutes, and then staining with hematoxylin and eosin (H&E, Solarbio, Beijing, China). After staining, excess stain was quickly removed, and the slides were sequentially immersed in 75%, 85%, 95%, and 100% ethanol (I) for 2-3 seconds each, followed by a 1-minute wash in 100% ethanol (II). Subsequently, the slides were cleared in xylene twice for one minute each time, mounted with neutral resin, and cover-slipped. The following day, observation and photography were conducted using a microscope (Leica Microsystems). (Cell nuclei were stained blue, while cytoplasm was stained pink to red).

4.15 Histological examination

The five major organs from the nude mice were fixed with 4% paraformaldehyde for 3-7 days, followed by paraffin embedding and sectioning (4 μm thick). The tissue slides were dewaxed and hydrated, subjected to antigen retrieval using sodium citrate, washed three times with PBS, treated with hydrogen peroxide to remove peroxidase, and then incubated in a humid chamber for 20 minutes. After washing with PBS, the slides were blocked with sheep serum for 20 minutes, followed by incubation with primary antibodies (Gli1: 1:1000, Proteintech, Beijing, China) at 4° C overnight. The next day, secondary antibodies (Solarbio, Beijing, China) were applied, followed by 1-hour incubation. DAB (1:50, Solarbio, Beijing, China) was used for color development, which was terminated with water after completion. Hematoxylin staining was performed, followed by dehydration and clearing. Finally, the slides were coverslipped for observation under a microscope.

4.16 Statistical analysis

Values are expressed as the mean ± standard error of the mean for three or more independent experiments, and were analyzed by GraphPad Prism software version 9.3. Student's t-test and analysis of variance (ANOVA) were used for assessment of statistical significance. $P<0.05$ represented a statistically significant difference.

Conflicts of interest

There are no conflicts to declare.

Acknowledgements

This work was supported financially by the National Natural Science Foundation of China (82003656), the Project of Science and Technology Department of Liaoning Province (2023-MS-328 and 2021-MS-351), General Project of Educational Department of Liaoning Province for Higher Education Institutions (LJKQZ2021178 and LJKZ1142) and Shenyang Young and Middle-aged Science and Technology Innovation Talent Support Program (RC210189).

References

[1]Q. Qin, R. Yu, J.E. Eriksson, H. Tsai, H. Zhu, Cancer-associated fibroblasts in pancreatic ductal adenocarcinoma therapy: challenges and opportunities, Cancer Lett. 591 (2024) 216859.

[2]O.T. Olaoba, T.I. Adelusi, M. Yang, T. Maidens, E.T. Kimchi, K.F. Staveley-O'Carroll, G.F. Li, Driver mutations in pancreatic cancer and opportunities for targeted therapy, Cancers 16 (2024) 1808.

[3]J. Kirkegård, C. Gaber, U. Heide-Jørgensen, C.W. Fristrup, J.L Lund, D. Cronin-Fenton, F.V. Mortensen, Effect of surgery versus chemotherapy in pancreatic cancer patients: a target trial emulation, J. Natl. Cancer Inst. (2024). DOI:10.1093/jnci/djae024

[4]H.Y. Duan, L. Li, S.M. He, Advances and prospects in the treatment of pancreatic cancer, Int. J. Nanomed. 18.(2023) 3973-3988.

[5]A.L. Lucas, M. Malvezzi, G. Carioli, E. Negri, C.L. Vecchia, P. Boffetta, C. Bosetti, Global trends in pancreatic cancer mortality from 1980 through 2013 and predictions for 2017, Clin. Gastroenterol. Hepatol. 14 (2016) 1452-1462.

[6]C.J. Halbrook, C.A. Lyssiotis, Employing metabolism to improve the diagnosis and treatment of pancreatic cancer, Cancer Cell 31 (2017) 5-19.

[7]S.P. Thayer, M.P. Magliano, P.W. Heiser, C.M. Nielsen, D.J. Roberts, G.Y. Lauwers, Y.P. Qi, S. Gysin, C.F. Castillo, V. Yajnik, B. Antoniu, M. McMahon, A.L. Warshaw, M. Hebrok, Hedgehog is an early and late mediator of pancreatic cancer tumorigenesis, Nature 425 (2003) 851-856.

[8]S.Y. Zhai, J.W. Lin, Y.C. Ji, R.H. Zhang, Z.H. Zhang, Y.Z. Cao, Y. Liu, X.M. Tang, J. Liu, P.Y. Liu, J.Y. Lin, F.L. Li, H.X. Li, Y.S. Shi, D. Fu, X.X. Deng, B.Y. Shen, A microprotein N1DARP encoded by LINC00261 promotes Notch1 intracellular domain (N1ICD) degradation via disrupting USP10-N1ICD interaction to inhibit chemoresistance in Notch1-hyperactivated pancreatic cancer, Cell Discovery 9 (2023) 95.

[9]W. Yan, R.E. Menjivar, M.E. Bonilla, N.G. Steele, S.B. Kemp, W.T. Du, K.L. Donahue, K.L. Brown, E.S. Carpenter, F.R. Avritt, V.M Irizarry-Negron, S. Yang, W.R. Burns, Y.Q. Zhang, M.P. Magliano, F. Bednar, Notch signaling regulates immunosuppressive tumor-associated macrophage function in pancreatic cancer, Cancer Immunol. Res. 12 (2024) 91-106.

[10]Y.Q. Zhang, J.P. Morris, W. Yan, H.K. Schofield, A. Gurney, D.M. Simeone, S.E Millar, T. Hoey, M. Hebrok, M.P. Magliano, Canonical wnt signaling is required for pancreatic carcinogenesis, Cancer Res. 15 (2013) 4909 – 4922.

[11]Z. Zhong, N. Harmston, K.C. Wood, B. Madan, D.M. Virshup, A p300/GATA6 axis determines differentiation and Wnt dependency in pancreatic cancer models, J Clin Invest. 132 (2022) e156305.

[12]M. Tsesmelis, U.F.G. Büttner, M. Gerstenlauer, U. Manfras, K. Tsesmelis, Z.W. Du, N. Sperb, S.E. Weissinger, P. Möller, T.F.E. Barth, H.J. Maier, L.K. Chan, T. Wirth, NEMO/NF-κB signaling functions as a double-edged sword in PanIN formation versus progression to pancreatic cancer, Mol. Cancer 23 (2024) 103.

[13]C. Yu, S.Y. Chen, Y.T. Guo, C.Y. Sun, Oncogenic TRIM31 confers gemcitabine resistance in pancreatic cancer via activating the NF-κB signaling pathway, Theranostics 8 (2018) 3224-3236.
[14]X. H. Shi, M. Wang, Y.Q. Zhang, X.J. Guo, M.Y. Liu, Z.J. Zhou, Y. Zhao, R.Z. He, Y. Gao, Y.H. Liu, S.T. Pan, M. Zhou, C.L. Zhao, T.Y. Yin, X. Li, H.B. Wang, J.X. Yang, F. Zhu, M. Li, R.Y. Qin, Hypoxia activated HGF expression in pancreatic stellate cells confers resistance of pancreatic cancer cells to EGFR inhibition, EBioMedicine 86 (2022) 104352.
[15]T. Qin, Y. Xiao, W.K. Qian, X.N. Wang, M.Y. Gong, Q.Q. Wang, R. An, L. Han, W.X. Duan, Q.Y. Ma, Z. Wang, HGF/c-Met pathway facilitates the perineural invasion of pancreatic cancer by activating the mTOR/NGF axis, Cell Death Dis. 13 (2022) 387.
[16]S.P. Pothula, Z.H. Xu, D. Goldstein, R.C. Pirola, J.S. Wilson, M.V. Apte, Targeting HGF/c-MET axis in pancreatic cancer, Int. J. Mol. Sci. 21 (2020) 9170.
[17]X.D. Kang, Z. Lin, M.H. Xu, J. Pan, Z.W. Wang, Deciphering role of FGFR signalling pathway in pancreatic cancer, Cell Proliferation 52 (2019) e12605.
[18]S. Nomura, H. Yoshitomi, S. Takano, T. Shida, S Kobayashi, M Ohtsuka, F. Kimura, H. Shimizu, H. Yoshidome, A. Kato, M. Miyazaki, FGF10/FGFR2 signal induces cell migration and invasion in pancreatic cancer, Br. J. Cancer 99 (2008) 305-313.
[19]G Feldmann, N. Habbe, S. Dhara, S. Bisht, H. Alvarez, V. Fendrich, R. Beaty, M. Mullendore, C. Karikari, N. Bardeesy, M.M. Ouellette, W. Yu, A. Maitra, Hedgehog inhibition prolongs survival in a genetically engineered mouse model of pancreatic cancer, Gut 57 (2008) 1420-1430.
[20]R. Jain, S. K. Dubey, G. Singhvi, The Hedgehog pathway and its inhibitors: Emerging therapeutic approaches for basal cell carcinoma, Drug Discovery Today 27 (2022) 1176-1183.
[21]V. Daggubati, A. Choudhury, A. Vykunta, O. Saulnier, Z. Gardell, J.Reiter, M.Taylor, D. Raleigh, CSIG-28. the hedgehog gene expression program regulates lipid feedback mechanisms underlying hedgehog-associated medulloblastoma, Neuro-Oncology, 24 (2022) vii45.
[22]T. Terao, Y. Minami, Targeting hedgehog (Hh) pathway for the acute myeloid leukemia treatment, Cells 8 (2019) 312.
[23]N. Fukushima, Y. Minami, S. Kakiuchi, Y. Kuwatsuka, F. Hayakawa, C. Jamieson, H. Kiyoi, T. Naoe, Small-molecule Hedgehog inhibitor attenuates the leukemia-initiation potential of acute myeloid leukemia cells, Cancer Sci. 107 (2016) 1422-1429.
[24]H. Deng, L. Huang, Z. Liao, M. Liu, Q. Li, R. Xu, Itraconazole inhibits the Hedgehog signaling pathway thereby inducing autophagy-mediated apoptosis of colon cancer cells, Cell Death Dis. 11 (2020) 539.
[25]T.Sheng, C. Li, X.Zhang, S. Chi, N. He, K. Chen, F. McCormick, Z. Gatalica, J. Xie, Activation of the hedgehog pathway in advanced prostate cancer, Mol. Cancer 3(2004)29.
[26]F. Galimberti, A. M Busch , F. Chinyengetere , T. Ma , D. Sekula , V.A. Memoli , K. H. Dragnev , F. Liu, K.C. Johnson, Y. Guo , S.J. Freemantle , A. S. Andrew, P. Greninger, D. J. Robbins, J. Settleman, C. Benes, E. Dmitrovsky, Response to

inhibition of smoothened in diverse epithelial cancer cells that lack smoothened or patched1 mutations, Int. J. Oncol. 41 (2012) 1751-1761.
[27]N. M. Nguyen, J. Cho, Hedgehog pathway inhibitors as targeted cancer therapy and strategies to overcome drug resistance, Int. J. Mol. Sci. 23 (2022) 1733.
[28]Y. Zhang, P. A. Beachy, Cellular and molecular mechanisms of hedgehog signalling, Nat. Rev. Mol. Cell Biol. 24(2023) 668–687.
[29]Z.F. Feng, S.S. Zhu, W.R. Li, M.J. Yao, H.L. Song, R.B. Wang, Current approaches and strategies to identify hedgehog signaling pathway inhibitors for cancer therapy, Eur. J. Med. Chem. 244 (2022) 114867.
[30]S. Hehlgans, P. Booms, Ö. Güllülü, R. Sader, C. Rödel, P. Balermpas, F. Rödel, S. Ghanaati, Radiation sensitization of basal cell and head and neck squamous cell carcinoma by the hedgehog pathway inhibitor vismodegib, Int. J. Mol. Sci. 19 (2018) 2485.
[31]D. Quatannens, Y.Verhoeven, P. V. Dam, F. Lardon, H. Prenen, G. Roeyen, M. Peeters, E. L. J. Smits, J. V. Audenaerde, Targeting hedgehog signaling in pancreatic ductal adenocarcinoma, Pharmacol. Ther. 236 (2022) 108107.
[32]D. Casey, S. Demko, S. Shord, H. Zhao, H. Chen, K. He, A. Putman, W. Helms, P. Keegan, R. Pazdur, FDA approval summary: sonidegib for locally advanced basal cell carcinoma, Clin. Cancer Res. 23 (2017) 2377–2381.
[33]M. R. Savona, D.A. Pollyea, W. Stock, V. G. Oehler, M. A. Schroeder, J. Lancet, J. McCloskey, H. M. Kantarjian, W. W. Ma, M . Shaik, A. D. Laird, M. Zeremski, A. O'Connell, G. Chan, J. E. Cortes, Phase Ib study of glasdegib, a hedgehog pathway inhibitor, in combination with standard chemotherapy in patients with AML or high-risk MDS, Clin. Cancer Res. 24 (2018) 2294–2303.
[34]R. M. Glasspool, S. P. Blagden, M. Lockley, J. Paul, C. Hopkins, F. Thomson, J. Brown, R. Fernandes, N. Douglas, C. Pou, A. Hanif, C. Campbell, P. S. Multani, T. Tucker, I. A. McNeish, T.R. J. Evans , A phase I trial of the oral hedgehog inhibitor taladegib (LY2940680) in combination with weekly paclitaxel in patients with advanced, solid tumours, J. Clin. Oncol. 35 (2017) doi:10.1200/JCO.2017.35.15_suppl.259
[35]C. A. Maschinot , L. Q. Chau , R. J. Wechsler-Reya , M. K. Hadden, Synthesis and evaluation of third generation vitamin D3 analogues as inhibitors of Hedgehog signaling, Eur. J. Med. Chem. 162 (2019) 495-506.
[36] Chun-Lan Li, Ze-Xuan Fang, Zheng Wu, Yan-Yu Hou, Hua-Tao Wu, Jing Liu, Repurposed itraconazole for use in the treatment of malignancies as a promising therapeutic strategy, Biomed. Pharmacother. 154 (2022) 113616
[37]S. Peukert , F. He , M. Dai , R. Zhang , Y. Sun , K. Miller-Moslin , M. McEwan , B. Lagu , K. Wang , Na. Yusuff , A. Bourret , A. Ramamurthy , W. Maniara , A. Amaral , A. Vattay , A. Wang , R. Guo , J. Yuan , J. Green , J. Williams , S. Buonamici , J. F. Kelleher , M. Dorsch, Discovery of NVP-LEQ506, a second-generation inhibitor of smoothened, ChemMedChem 8 (2013)1229-1229.
[38]A. D. Jesus-Acosta, E. A. Sugar, P. J. O'Dwyer, R. K. Ramanathan, D. D. V. Hoff, Z. Rasheed, L. Zheng, A. Begum, R. Anders, A. Maitra, F. McAllister, N. V. Rajeshkumar, S. Yabuuchi, R. F. de Wilde, B. Batukbhai, I. Sahin, D. A. Laheru, Phase

2 study of vismodegib, a hedgehog inhibitor, combined with gemcitabine and nab-paclitaxel in patients with untreated metastatic pancreatic adenocarcinoma, Br. J. Cancer 122(2020) 498–505.
[39]D. V. T. Catenacci, M. R. Junttila, T. Karrison, N. Bahary, M. N. Horiba, S. R. Nattam, R. Marsh, J. Wallace, M. Kozloff, L. Rajdev, D. Cohen, J. Wade, B. Sleckman, H. Lenz, P. Stiff, P. Kumar, P. Xu, L. Henderson, N. Takebe, R. Salgia, X. Wang, W. M. Stadler, F. J. de Sauvage, H. L. Kindler, Randomized phase ib/ii study of gemcitabine plus placebo or vismodegib, a Hedgehog Pathway Inhibitor, in Patients With Metastatic Pancreatic Cancer, J. Clin. Oncol. 33 (2015) DOI:10.1200/JCO.2015.62.871
[40]A.L. McCleary-Wheeler, R.M. Carr, S. R. Palmer, T. C. Smyrk, J. B. Allred, L. L. Almada, E. J. Tolosa, Maria J. Lamberti, David L. Marks, Mitesh J. Borad, Julian R. Molina, Yingwei Qi, Wilma L. Lingle, A. Grothey, H. C. Pitot, A. Jatoi, D. W. Northfelt, A. H. Bryce, R. R. McWilliams, S. H. Okuno, P. Haluska, G. P. Kim, G. Colon-Otero, V.J. Lowe, M. R. Callstrom, W. W. Ma, T. Bekaii-Saab, M. Hung, C. Erlichman, M.E. Fernandez-Zapico, Phase 1 trial of vismodegib and erlotinib combination in metastatic pancreatic cancer, Pancreatology(2020) 101-109.
[41]J. Wang,Y. Zhang,W. Huang, J.Yang,W. Tang, T. Huang, W. Tan, ABT-199 inhibits hedgehog pathway by acting as a competitive inhibitor of oxysterol, rather as a BH3 mimetic. Acta Pharmacol. Sin. 42(2021) 1005–1013.
[42]R. L. Yauch, G. J. P. Dijkgraaf, B. Alicke, T. Januario, C. P. Ahn, T. Holcomb, K. Pujara, J. Stinson, C. A. Callahan, T. Tang, J. F. Bazan, Z. Kan, S. Seshagiri, C. L. Hann, S. E. Gould, J. A. Low, C. M. Rudin, F. J. de Sauvage, Smoothened mutation confers resistance to a hedgehog pathway inhibitor in medulloblastoma, Sci. 326 (2009) 572-574.
[43]B. T. Baby , A. M. Kulkarni , P. K. R. Gayam , K. B. Harikumar , J. M. Aranjani, Beyond cyclopamine: targeting hedgehog signaling for cancer intervention, arch. biochem. biophys. 754 (2024)109952.
[44]L. L. Siu , K. Papadopoulos , S. R. Alberts , R. Kirchoff-Ross , B. Vakkalagadda , L. Lang , C. M. Ahlers , K. L. Bennett , J. M. Van Tornout, A first-in-human, phase I study of an oral hedgehog (HH) pathway antagonist, BMS-833923 (XL139), in subjects with advanced or metastatic solid tumors. J. Clin. Oncol. 28 (2010)DOI:10.1200/jco.2010.28.15_suppl.2501
[45]N. P. Shah, J. E. Cortes, G. Martinelli, B. D. Smith, E. Clarke, M. Copland, L. Strauss, M. Talpaz, Dasatinib plus smoothened (smo) inhibitor BMS-833923 in chronic myeloid leukemia (CML) with resistance or suboptimal response to a prior tyrosine kinase inhibitor (TKI): phase I study CA180323, Blood 124 (2014) 4539.
[46]S. M. Roopan, R. Sompalle, Synthetic chemistry of pyrimidines and fused pyrimidines: A review, Synth. Commun. 46(2016) 645-672.
[47]J. S. Cruz, A. P. de Aguiar, Overview of the biological activities of pyrimido[4,5-d]pyrimidines. Mini-Rev. Med. Chem. 21 (2021) 2138-2168.
[48]M. Tokuhira, Y. Kimura, K. Sugimoto, T. Nakazato, M. Ishikawa, I. Fujioka, T. Takaku, N. Iriyama, E. Sato, H. Fujita, Y. Hatta, N. Komatsu, N. Asou, M. Kizaki, T.

Kawaguchi, Efficacy and safety of nilotinib therapy in patients with newly diagnosed chronic myeloid leukemia in the chronic phase. Med. Oncol. 35 (2018) 1-8.
[49]S. Park, E. A. Cho, J. N. Chun, D. Y. Lee, S. Lee, M. Y. Kim, S. M. Bae, S. I. Jo, S. H. Lee, H. H. Park, T. M. Kim, I. So, S. Y. Kim, J. Jeon, Exp. Mol. Med. 54 (2022) 1225-1235.

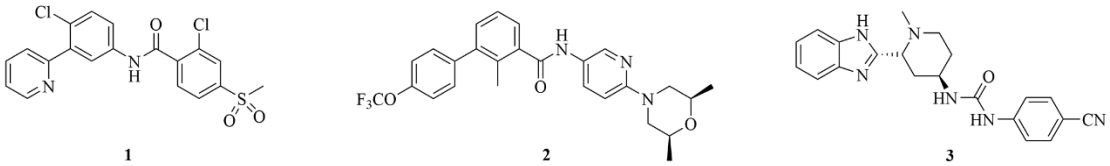

Figure 1

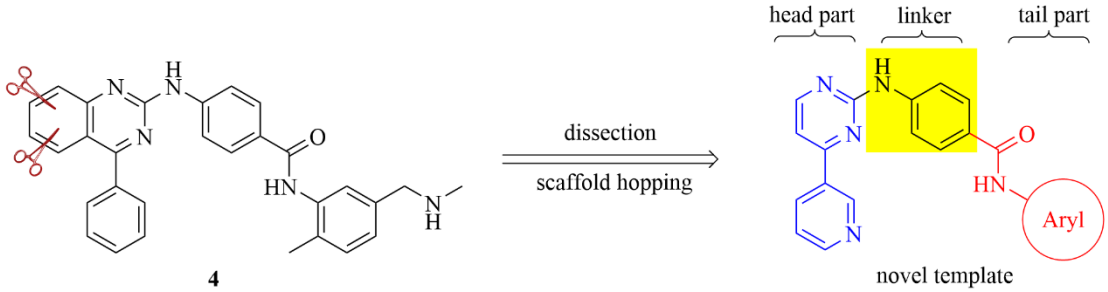

4

Figure 2

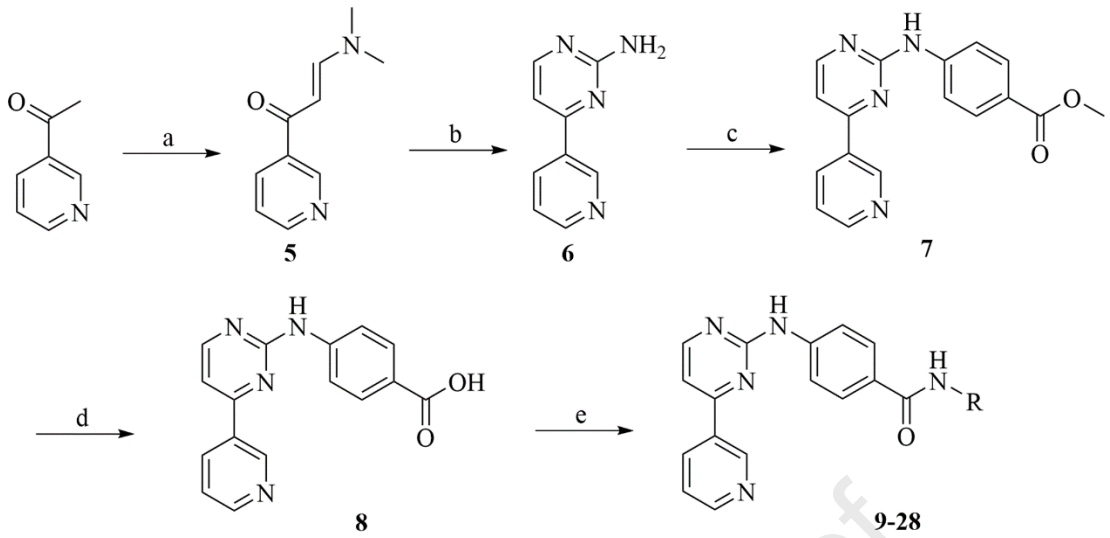

Scheme 1

Table 1 Structure activity relationship (SAR) of target compounds

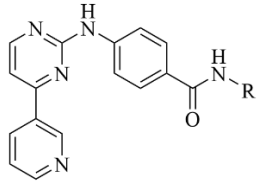

Compd.	R	Gli-luc reporter IC_{50}[a](nM)	Compd.	R	Gli-luc reporter IC_{50}[a](nM)
9	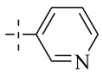	28.1 ± 3.1	20	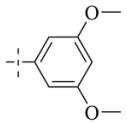	29.7 ± 2.9
10	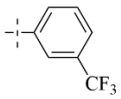	25.6 ±2.7	21	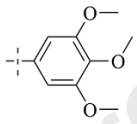	18.6 ± 1.7
11	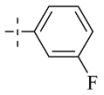	15.9 ± 1.8	22	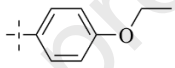	12.2 ± 0.9
12	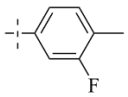	46.4 ± 5.2	23	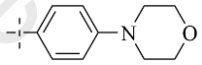	17.3 ± 1.6
13	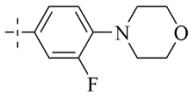	33.5 ± 4.5	24	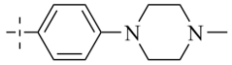	4.5 ± 0.4
14	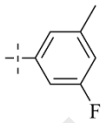	10.3 ± 0.7	25	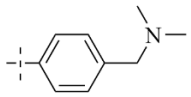	2.7 ± 0.2
15	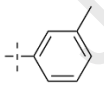	13.8 ± 1.5	26	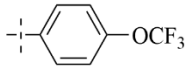	ND
16	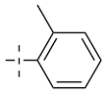	14.6 ± 1.2	27	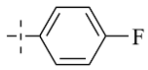	35.3 ± 4.8
17	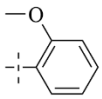	9.1 ± 0.4	28	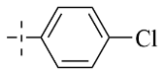	24.8 ± 2.9
18	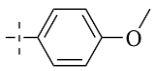	14.2 ± 1.0	4		5.5 ± 0.6
19	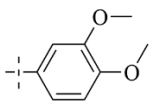	22.5 ± 2.3	1		15.1 ± 1.1

[a]IC_{50} denote the drug concentration that inhibits 50% of Gli-luc reporter. Values are expressed as the mean ± standard error of the mean for three independent experiments. ND means not determined.

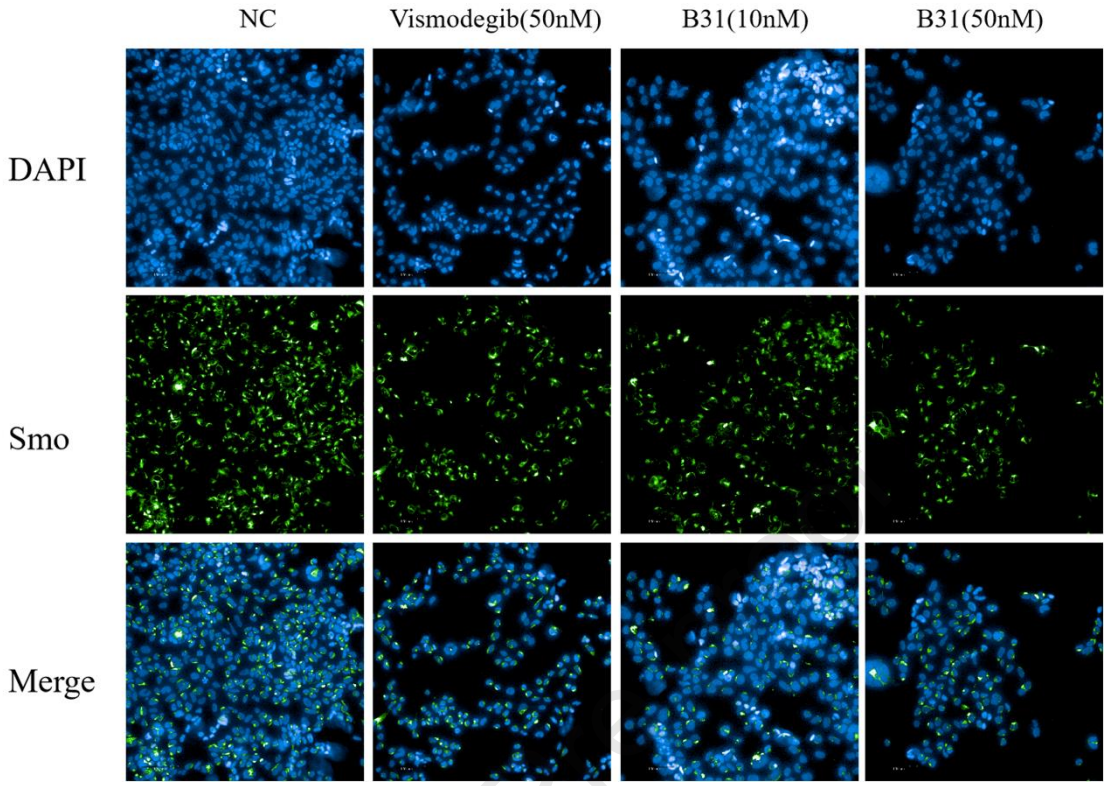

Figure 3

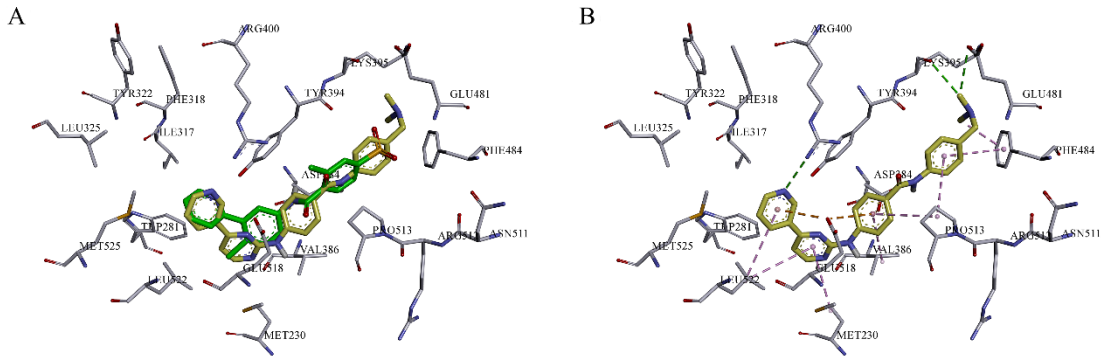

Figure 4

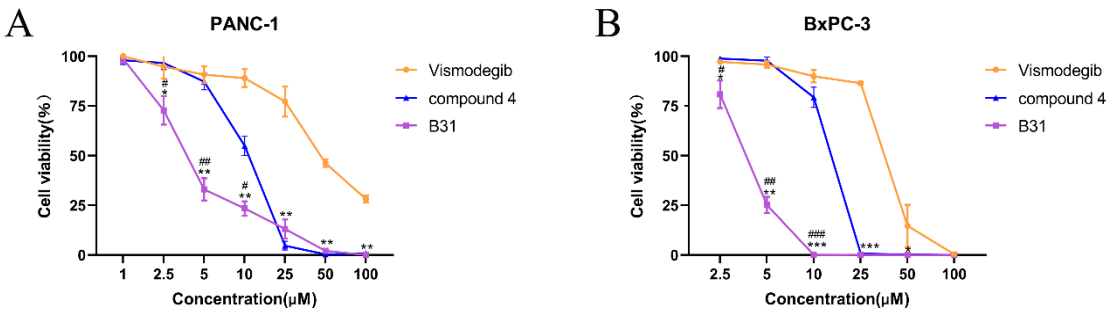

Figure 5

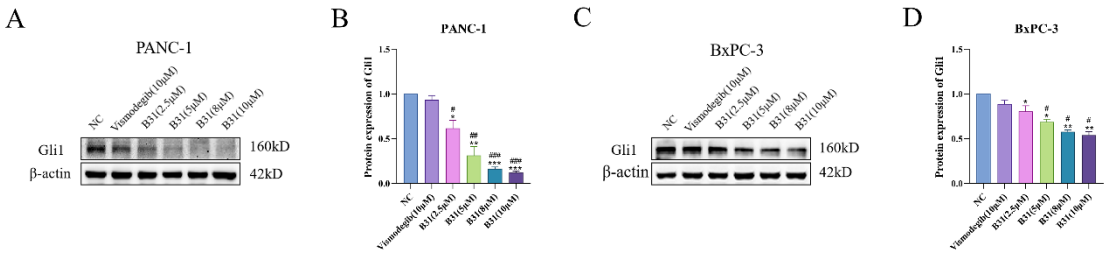

Figure 6

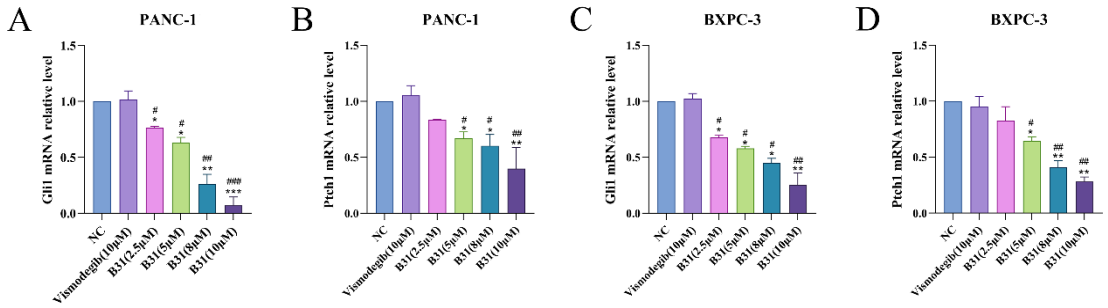

Figure 7

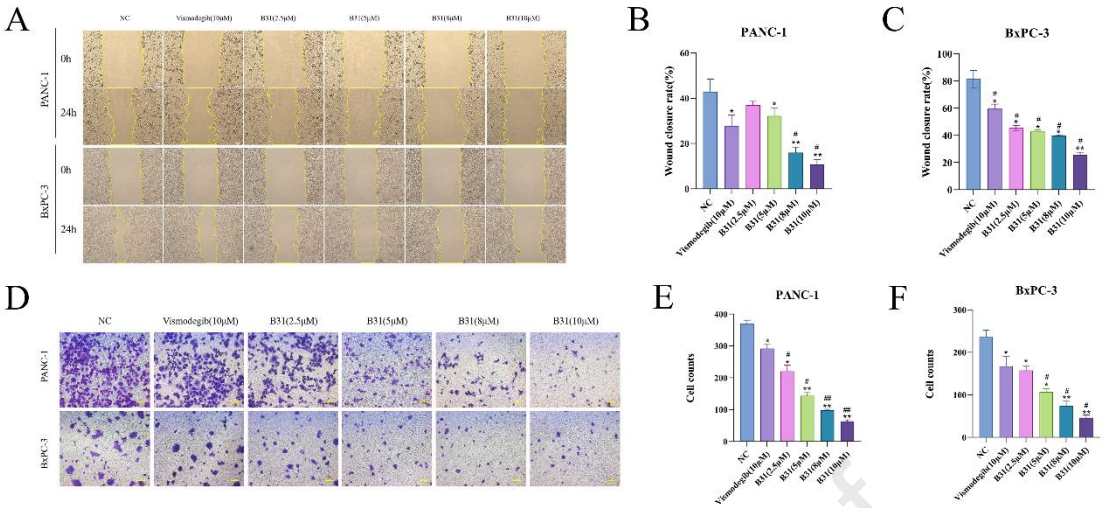

Figure 8

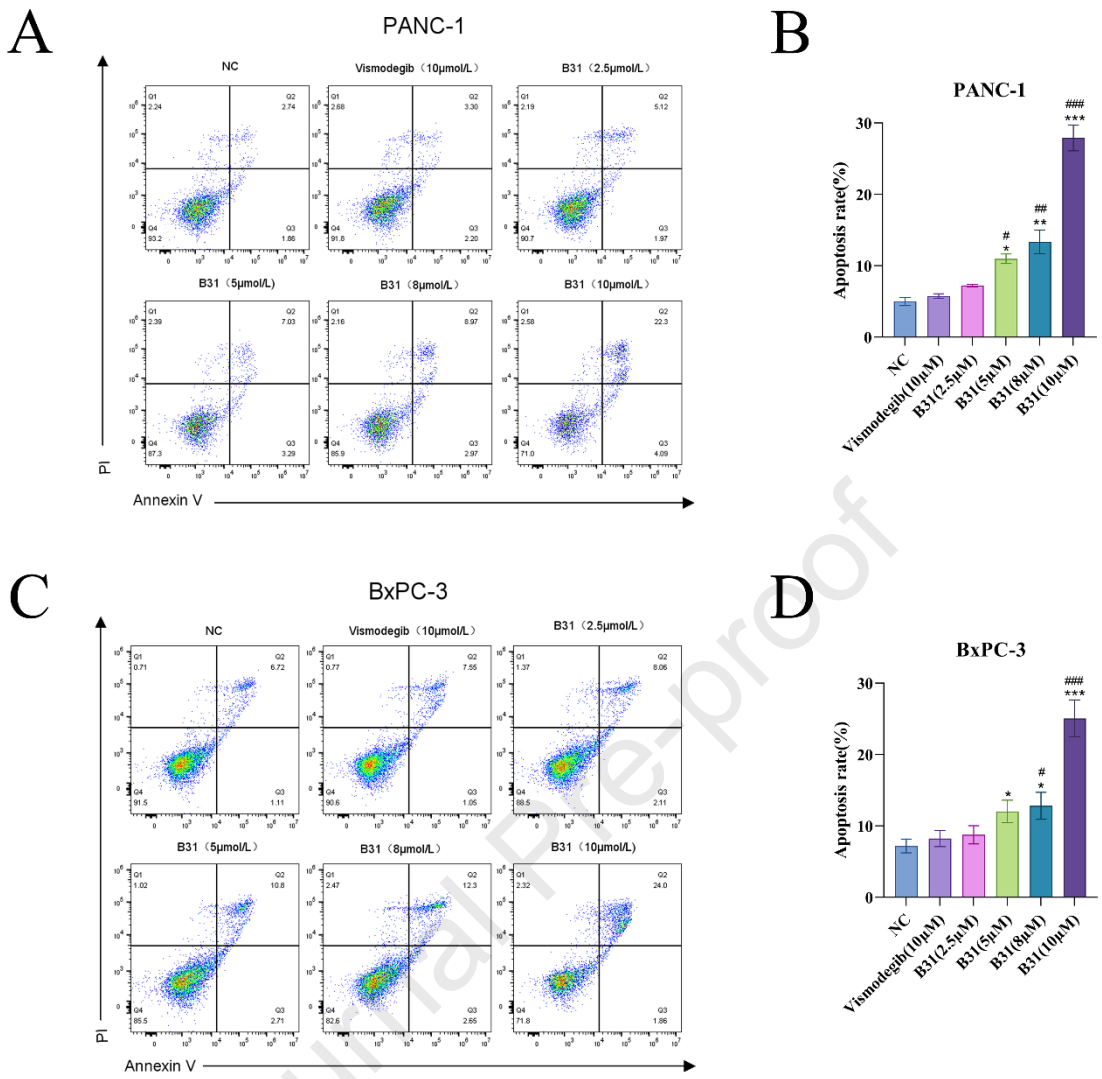

Figure 9

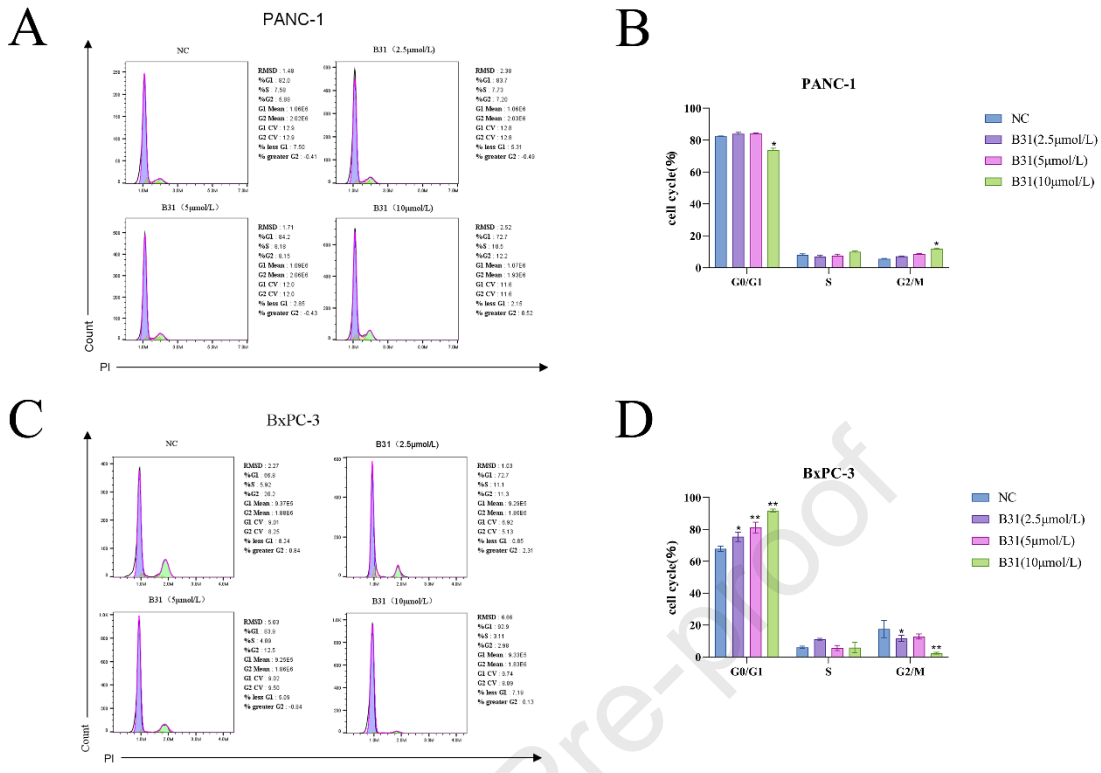

Figure 10

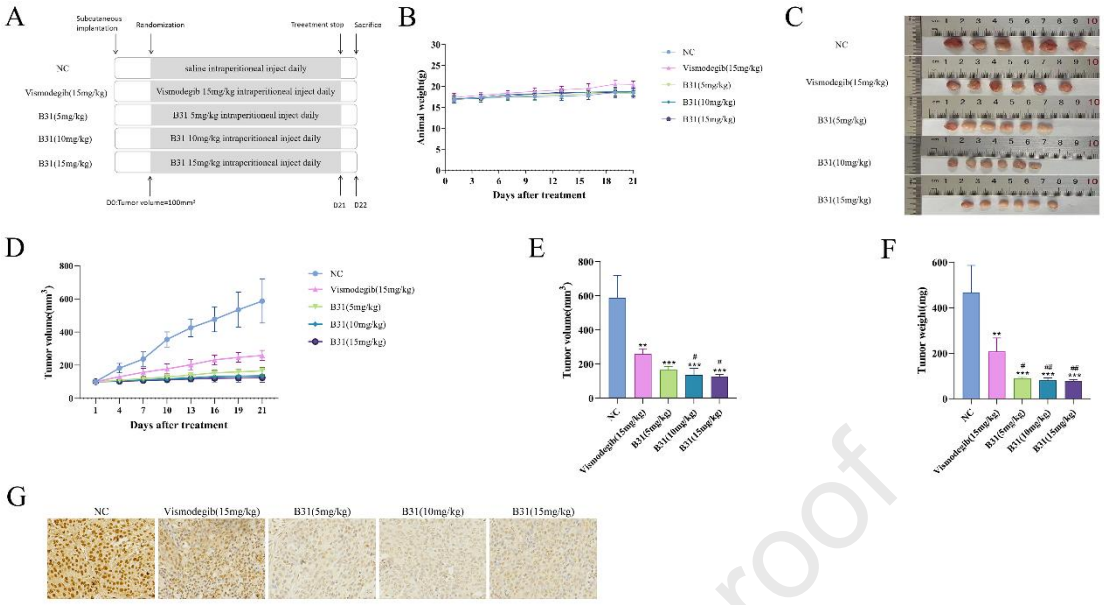

Figure 11

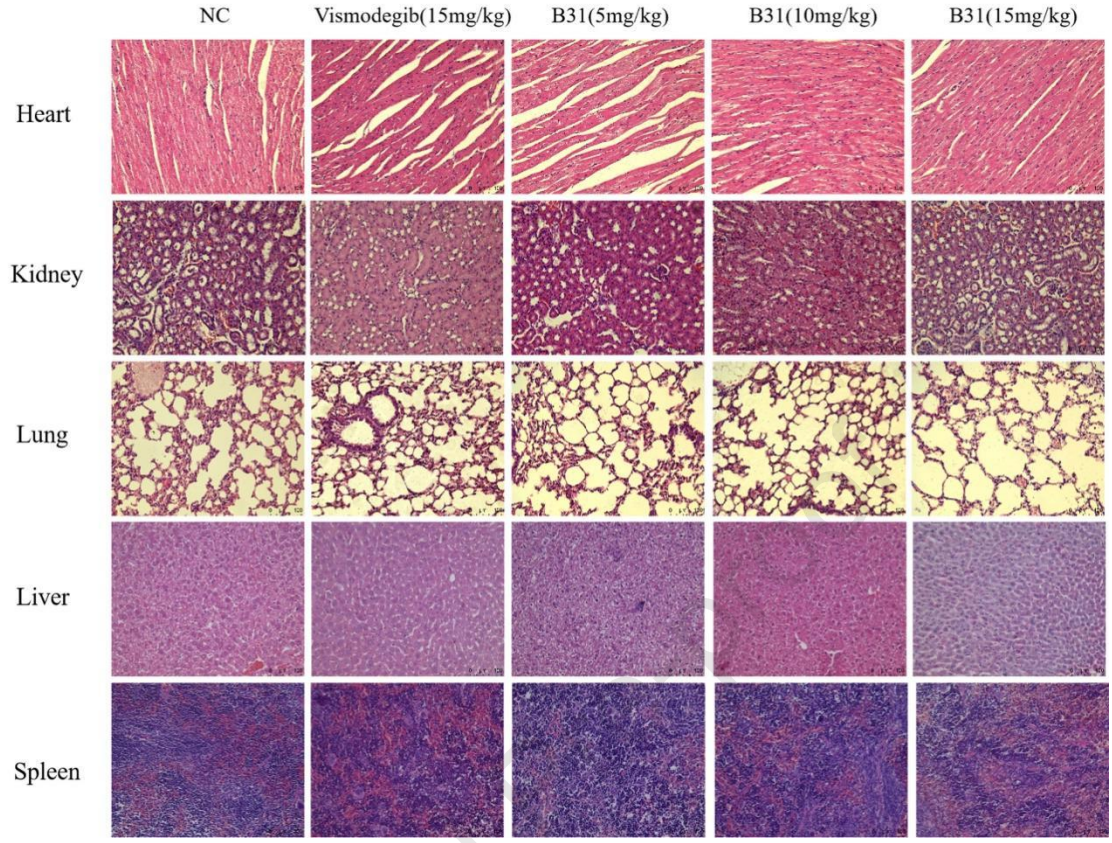

Figure 12

Highlights

1. A series of novel pyridyl pyrimidine hedgehog inhibitors were synthesized and evaluated.

2. The computational simulation revealed the preferential inhibition of Smo by Compound **25** (B31) at the molecular level.

3. B31 not only exhibited antiproliferative effect on various pancreatic cancer cell lines but also significantly inhibited pancreatic tumor growth.

Conflicts of interest

There are no conflicts to declare.